DOSE-EFFECT RELATIONSHIPS FOR ULTRASOUND IRRADIATION OF BRAIN TISSUE

BY

RONALD LEE JOHNSTON

B.S., University of Illinois, 1973

THESIS

Submitted in partial fulfillment of the requirements
for the degree of Doctor of Philosophy in Biophysics
in the Graduate College of the
University of Illinois at Urbana-Champaign, 1979

Urbana, Illinois

DOSE-EFFECT RELATIONSHIPS FOR ULTRASOUND IRRADIATION OF BRAIN TISSUE

Ronald Lee Johnston, Ph.D.

Department of Physiology and Biophysics

University of Illinois at Urbana-Champaign, 1979

A series of experimental animals were irradiated using high-intensity focused ultrasound in the frequency range from 1 to 7 MHz to produce irreversible structural alterations in brain tissue (surgical focal lesions). A dose-effect relationship was demonstrated to exist between the calculated absorbed energy per unit volume, expressed as joules/mm^3, and the volume of the produced lesions as measured on histologically prepared tissue sections. It was also shown that equal size lesions, produced at a given dose-rate or intensity, were obtained at two different ultrasound irradiation frequencies by equivalent values in absorbed dose.

Another series of experiments were conducted to study the effects of the superior brain meninges (dura mater, arachnoid membrane, and pia mater) on the propagation of ultrasound to investigate the apparent frequency dependence, over the range of 1 to 9 MHz, in the minimum irradiation exposure required for the just discernable appearance of a brain lesion as evidenced by subsequent histological preparation and optical microscopy (an apparent threshold phenomenon). A model of the meningeal layers involving different propagation properties due to collagenous inclusions was found to fit the data of previous investigators and was found to predict behavior which was subsequently tested by irradiations at 7 MHz. This mathematical description provides a means to refine estimates

of intensities delivered to the irradiation sites in brain tissue.

Hysteresis associated with the non-linear stress-strain response of tissues subjected to high levels of stress at ultrasonic frequencies was considered as an ultrasound-tissue interaction mechanism for the production of the irreversible structural biological effects. Thus, hysteresis was found capable of describing accurately the previously observed "threshold" curve for this endpoint. This mechanism was considered in its relationship to other proposed tissue interaction mechanisms of ultrasound. Hysteresis predicted other observable ultrasonic effects which were listed as possible areas of future research. Hysteresis effects in tissues included non-linear or intensity dependent acoustical absorption coefficient, linearly increasing absorption coefficient with increasing frequency, dispersion-free velocity, and harmonic production. Partial evidence for these effects were cited from works of other experimenters.

ACKNOWLEDGEMENT

The author wishes to express his appreciation to his advisor, Professor Floyd Dunn, for suggesting the research topic, and for his encouragement and guidance through its completion. Special thanks are offered to members of the Thesis Advisory Committee: Dr. Floyd Dunn, Professor of Electrical Engineering, Physiology and Biophysics, Dr. William D. O'Brien, Jr., of the Department of Electrical Engineering, and Dr. Howard S. Ducoff, Professor of Bioengineering, Physiology, and Biophysics.

The author wishes to thank Mrs. Wanda Elliott for her assistance in typing the manuscript. And special appreciation is offered for the continual encouragement and support from the author's wife, Roberta.

This research was supported in part by the National Science Foundation grants NSF ENG 74-14095 and 77-20934.

TABLE OF CONTENTS

Chapter 1

INTRODUCTION

With regard to biological systems, ultrasound may be somewhat unique among the several various forms of radiant energy available for interaction. Biological systems have evolved in the continued presence of natural forms of radiation such as low levels of particulate ionizing radiation, as well as, electromagnetic forms varying from gamma and X-rays to ultraviolet light. Even non-ionizing radiation due to microwave and radio frequency waves werecontinually present during evolutionary periods but at what are considered biologically insignificant levels for affecting changes in biological structure and function. Many life forms developed protective measures and repair mechanisms for these background level radiation exposures and the bioeffects they produced. However, ultrasound in the frequency range of several hundred kilohertz to several hundred megahertz is a man made form of mechanical energy which very likely had no previous environmental influence on biological evolution. Since the benefits from the use of low level megahertz ultrasound in medical diagnostics far outweigh any presently known risks, the clinical use of ultrasound is proliferating at a rapid rate (Smith, 1976). Hence, the study of ultrasound and its interactions with biological materials is deemed essential for a complete understanding of the physical mechanisms of interaction and also for the assessment of any possible risk which may be associated with human exposure under these conditions.

The importance of this later goal is demonstrated by the rapid growth of ultrasonic visualization techniques in medical diagnosis (O'Brien, 1978). In obstetrics, for example, ultrasound has virtually replaced X-ray procedures as

the diagnostic modality of choice for *in utero* fetal assessment (Marx, 1974). In some hospitals and clinics it has become standard procedure for the physician to order some form of ultrasound examination in the course of a pregnancy even when no indications exist for its need. It is possible that a fetus could undergo one or all of the following procedures in the course of its development; multiple ultrasound Doppler examinations during early pregnancy to detect fetal heart motion, scans for fetal cephalometry to determine gestational age or rate of growth, ultrasound examinations for gross abnormalities such as spina bifida, hydrocephalus, or anencephaly, ultrasound scans for possible mutilple pregnancies, ultrasound guided amneocentesis and placental localization, and fetal heart monitoring for long durations during labor (Brown, 1971). Since the rapidly developing and differentiating cells of a fetus may be the most vulnerable to disturbances in development due to exogenous influences, a prime area for research in ultrasound bioeffects has been fetal toxicity and teratology. No fetal toxic or teratogenic effects have been observed except at intensity levels far above those used diagnostically (Fry et al., 1977).

Ultrasound diagnostic procedures are used to examine virtually all organs of the body in neonates and adults. The use of ultrasound for cardiovascular assessments has proved to be an invaluable tool (Brown, 1971). Next to obstetrical procedures, cardiovascular diagnostics has made the greatest use of the developing ultrasound technologies. Time and motion studies of the dynamic action of the heart walls, valves, and outflow characteristics as well as Doppler flow studies on the peripheral vascular system have shown that the beneficial uses of ultrasound as a diagnostic and research tool are developing at a rate that far exceeds research on possible biological hazards of ultrasound as used at diagnostic

levels (Brown, 1971; Stratmeyer, 1977).

Above the ultrasound intensities used at diagnostic levels, and in the range of 1 to 10 W/cm^2, ultrasound is used medically for its therapeutic effect, chiefly as a diathermy modality on the extremities and on major muscle groups (Lehmann and Guy, 1972). At these intensity levels, numerous biological effects have been noted and physicians observe certain contraindications for its use. For example, ultrasound diathermy is to be avoided where residual radiation may impinge on the gravid uterus (Lehmann et al., 1978). Mostof the observed biological effects of ultrasound at levels of 10-100 W/cm^2 can be explained on the basis of the thermal changes produced by absorption of ultrasound energy in the tissues involved. However, some biological effects at these intensity levels which have been observed cannot be explained in terms of only a thermal mechanism. For example, Nyborg (1978) has cited the following experimental observations where non-thermal modes may have had some part in the results; changes in the electrophoretic mobility of irradiated Ehrlich cells migrating in an electric field, changes in transport across membranes, destruction of lysosomes in irradiated liver tissue, alterations of mitochandria in liver, muscle, and kidney, decreases in the number of glycogen granules in exposed liver tissue, and changes in cell division processes.

At intensities of 50-1000 W/cm^2 and above, ultrasound has been used as a surgical tool on patients for the treatment of Meniere's disease (Kossoff et al., 1966) and for neurosurgery to destroy specific brain sites for relief of hyperkinetic movement disorders (Meyers et al., 1959). It is at these very high intensity levels that the greatest volume of data on reproducible biological effects of ultrasound on animals and man exists for which likely mechanisms of interaction have been identified. Having made suitable determinations for the threshold exposure conditions for the observed cellular changes, it is possible to further

our understanding of existing modes of tissue interactions and it is possible to establish dosage criteria for better specifying conditions of ultrasound exposure.

1.1 Dosimetry

Inherent in the establishment of a dosimetric quantity, a quantity that is descriptive and useful for dealing with an observed biological effect, is the complete quantitative specification of the external physical exposure parameters necessary to elicit the phenomenon. Then, in order to establish a dose-effect relationship, it is necessary to show a graded tissue response as a function of variations of the applied exposure dose. Then, knowledge of the mechanisms of tissue interactions allows for dosage quantities to be specified in terms of that portion of the total exposure dose responsible for the observed bioeffects, which is usually expressed as an absorbed dose. Ultrasound radiation dosimetry has followed a course similar to that taken by the field of ionizing radiation biophysics, in the past, by specifying exposure parameters for biological effects in terms of an externally applied "exposure dose." In the case of ultrasound, this has traditionally been expressed in terms of an exposure dose-rate such as watts per square centimeter. Later dosimetric refinements in ionizing radiation dosimetry have shown that bioeffects due to ionizing radiation are better specified in terms of "dose equivalents" which combine the concept of absorbed dose and a quality factor which represents the relative biological effectiveness of the applied radiation in terms of its energy and composition. Also included are other modifying factors due to energy density and mode of dose fractionation. Such a dosimetric quantity allows a broad range of biological effects to be meaningfully compared based on dose.

1.2 Statement of Thesis and Content

In order to investigate dosimetric relationships for high intensity ultrasound bioeffects, work was undertaken as described in Chapter 4, based on the experimental procedures of Chapter 3, to study an approximation to absorbed dose, dose rate, and their effect on the produced lesion volume in brain tissue irradiated by focused ultrasound. Based on the dose-effect relationship of absorbed energy per unit volume of irradiated tissue and produced lesion volume which was observed, a comparison of effects at 3 and 4 MHz was made. The work which was conducted showed absorbed energy per unit volume, expressed as joules per cubic millimeter, to be an appropriate dosimetric quantity for the observed bioeffect of produced lesion volume for a given exposure dose rate. Chapter 5 describes experiments conducted to investigate the frequency effects on observed threshold lesion behavior due to the ultrasonic propagation properties of the superior brain meninges. The results of this section allow for additional refinement in exposure dose parameters by correcting for tissue effects on the ultrasonic intensity delivered to the irradiated site. Chapter 6 contains a discussion of mechanisms of ultrasound bioeffects at surgical level intensities and sets forth a proposed additional physical mechanism based on hysteresis loss due to the non-linear stress-strain response of tissue. The proposed model is examined with regard to presently accepted modes of tissue interactions at levels of irradiation intensities above and below the range for which the model is proposed. Physically observable consequences of the tissue non-linearities are examined and examples of their possible observation by others are listed. Suggested areas for future research are also offered.

Chapter 2

EXPERIMENTAL METHODS

2.1 Ultrasonic Irradiation Equipment and Calibration

The exposure instrumentation, calibration procedure, and its use in the experimental animal irradiation has been extensively described elsewhere by Fry et al. (1954, 1955), Barnard (1955, 1956), and Fry and Dunn (1962). The following is a brief description of these procedures. A rectangular envelope pulse of a chosen time duration and fixed rf frequency is amplified and supplied to a series capacitor voltage divider which is capable of supplying the desired calibrated voltage to a focused ultrasound transducer. The ultrasound output of the transducer is calibrated each day prior to the experimental animal preparation and exposure by the use of a calibrated transfer standard consisting of a thermocouple enclosed in oil (Fry and Dunn, 1954a,b). The thermocouple standard is itself calibrated for each frequency of interest with a known ultrasonic intensity, plane-wave field in a calibration tank. Prior to calibrating the thermocouple, the ultrasonic intensity of the field in the calibration tank is determined by a suspended sphere radiometer (Dunn and Fry, 1971) which measures the radiation pressure of the traveling acoustic wave (Fox, 1940; Hasegawa and Yosioka, 1969). As a primary standard, this technique allows for an accuracy of $\pm 3\%$ in intensity determination. Even though variations in the exposure calibration of the output of the transducer used for experimental animal irradiations is less than 5% over several months time, complete beam plots and thermocouple calibrations are performed prior to each experiment to verify transducer irradiation output calibration and beam profile.

2.2 Organ Choice for Irradiations

The brain has been the organ of choice for ultrasound lesion threshold experiments due to the virtual lack of dependence of the acoustic parameters of absorption, velocity, and impedance, on such functional characteristics as diet, animal weight, past and current health status, and possible drug therapy effects on tissue physiology, etc. Such considerations which can affect other organs, such as liver and muscle, have no significant effect on the ultrasonic properties of brain tissue (Quastel, 1961). This may be due to the post-mitotic nature of C.N.S. tissue and to the relative impermeability of the blood-brain barrier to commonly used antibiotic drugs. In addition, those disease states which could affect the acoustic properties of the brain are usually pathologies which tend to cause gross anatomical changes which would be evidenced by obvious animal degeneration (Quastel, 1961). Animals displaying anomalous behavior such as adipsia, ataxia, and aphagia were considered unsuitable for this study. Animals which were found to be diseased at autopsy were so noted and the data discarded if the subsequent histological examination of the brain tissue showed any pathological effects such as cerebral wasting, anomalous blood or CSF extravasation, lesions due to disease, or brain shape distortion.

2.3 Experimental Animal Species Selection

The animal of choice for stereotaxic neurosurgical procedures is the adult female cat (*Felis domesticus*). This animal, which is a readily available, medium sized mammal, exhibits the least variability with respect to skull bone thickness, cranial vault dimensions, brain volume, and inter-breed differences. This negligible amount of major anatomical variation allows for a high degree of reproducibility in sterotaxic localization of specific brain sites. The relative constancy that exists between external skull landmarks and internal brain structures, in

addition to the uniform size and brain shape allows for anatomic localization to within ±0.5 mm at any desired irradiation site (Jasper and Ajmone-Marson, 1960). The Siamese breed is excluded from these considerations as these cats exhibit marked differences in brain anatomy in the areas of the corpus callosum and optic pathways.

2.4 Stereotaxic Technique

The stereotaxic method employed is basically that introduced by Horsley and Clark (1908). The subsequent elaboration and refinements of Clark (1920) and Ingram, Hannett, and Ranson (1932) have been employed.

The head of the anesthetized animal is affixed to a rigid stereotaxic frame by means of four locating bars which establish the three-dimensional sterotaxic reference planes. Two ear bars, one in each external auditory meatus, establish a vertical, or frontal, plane at what is defined as "ear-bar zero." Two notched locating bars are positioned over the infra-obital ridges of the eyes. The infra-orbital ridges, in conjunction with the ear-bar points, establish a horizontal, transverse, or Frankfurt plane. However, more recent convention has established that the zero plane of reference shall be the plane 1 cm above the horizontal plane which Horsly and Clarke (1908) originally designated (Jasper and Ajmone-Marson, 1960). The median plane is located at one-half the distance between the ear-bars and coincides with the mid-sagittal planes of the animal.

The animal's trunk is supported ventrally in a semi-circular, copper jacketed, water-heated belly-pan, which attaches to the stereotaxic frame. The heated pan aids in controlling the animal's body temperature to eliminate the hypothermia characteristic of deep anesthesia.

2.5 Surgical Preparation

2.5.1 Presurgical Procedures

At least 18 hours before surgery, food and water are withdrawn to minimize the possibility of respiratory complications, should the anesthetized animal aspirate regurgitated stomach contents. The experimental animal is wieghed and the anesthetic dosage is determined at a rate of 1 ml per kg body weight sodium pentobarbital (1 grain per ml) (Siegmund, 1961). The drug is injected intraperitoneally. Due to the variability of individual animal response to anesthetic agents, especially when given intraperitoneally, the depth of anesthesia is assessed by corneal reflex response or carpal-pedal response. If after 20-30 minutes, the depth of anesthesia is not sufficient, a second dose, half the previous injection, is given. Animals displaying laryngeal, or bronchial spasms, or copious salivation may require 1/150 grain of atropine sulfate.

After the animal has reached the required degree of anesthesia, the head is shaved between the ears from the region above the frontal sinuses to the nape of the neck. The auditory canals are cleansed and swabbed with mineral oil and the animal is then placed in the stereotaxic frame. The ear-bars are inserted first. The positioning of the ear-bars is of primary importance for successful use of the stereotaxic procedure and great care must be taken to insure precise placement. The head must show rigid fixation for any movements against the ear-bars and free movements about the axis of the ear-bars. The jaw should be capable of being moved through its normal range of movement, indicating no mandibular obstruction by incorrect placement of the ear-bars such as, into the mandibular notches. The head is then centered by adjusting the ear-bars for equal displacement indicated by the calibrated verniers on the frame.

The infra-orbital ridges are located and notched bars are affixed. An

additional notched bar is fitted from below, to apply upward pressure against the upper incissors, thus locating the head firmly against the infra-orbital bars.

2.5.2 Surgical Procedure

A midline incision approximately 75 mm in length is made from the area above the frontal sinus to the area above the cerebellum. The sub-scalp membranous attachments to the skull are freed and the scalp is retracted laterally by the weight of hemostats applied to the underside of the scalp in order to avoid damage to the area of the incised tissue. The temporalis is cut along its origin, and as close to the origin as possible to minimize bleeding, and scraped laterally with a gauze wrapped blunt instrument.

The frontal sinuses are opened with a 1 cm trephine and further exposed with bone cutters. The sinuses are cleared and packed with bone wax to minimize loss of the physiological saline used for conducting the ultrasound to the brain during the ultrasonic irradiation procedure.

A series of three 1 cm trephinations are made on each side of the skull. Dural attachments to the skull are freed around the area of each opening and Rongeur forceps are used to remove bone between the trephined holes. Bleeding is controlled with bone wax. Great care is taken not to injure the dura-mater in any way, which minimizes the chance of infection and preserves the uniformity of the experimental animal preparation.

After sufficient bone removal around the periphery of the cut edge of the skull, the superior portion of the calvarium may be removed by careful lifting and separating of bone from the dura-mater below. Dural elevators or dental spatulas may be used to free the dural attachments to the skull and to minimize its tearing. Any bleeding is controlled by oxidized, regenerated cellulose and

bone wax.

The surgical field is then cleared of bone fragments and any other extraneous material which would interfere with the sound field propagation. The stereotaxic frame is fitted on locating pins on the base of the irradiation platform and locked into place.

The surface topography of the brain, over the selected irradiation sites, is measured by just bringing into contact with the brain surface a stainless steel pointer, attached to the transducer, which indicates the location of the center of the focal volume of the transducer. These vertical position measurements are used to calculate the depth of the selected irradiation site, which is then used to make a first order correction on the ultrasonic exposure intensity in order to compensate for the attenuation of the intervening brain tissue. A computer program determines the settings for the rf generator output, based on the desired intensity to be delivered to the site of interest, the depth of the site, the attenuation of the tissue at the frequency being used, and the transducer output calibration determined earlier that day.

The surgically prepared and stereotaxically mounted animal is further prepared for irradiation by affixing a head-pan, of about nine liter capacity, to the scalp. A water tight seal is made, between the scalp and the pan, by compressing the scalp opening to the opening in the pan by means of a stainless steel wire tourniquet. Approximately seven liters of degassed, sterile, physiological saline at 37^{o}C is used to fill the head pan, which couples the sound beam from the transducer to the brain.

A needle thermistor is inserted near the medulla to monitor brain temperature and to drive a temperature controller which heats the physiological saline in the head pan. Body temperature is measured rectally and is maintained by circulation

of heated water in the copper-clad belly support structure. Additional body heat, when required, is supplied by an electrically heated pad placed over the animal. About 15 to 20 minutes are allowed for temperature stabilization of the specimen to become established, prior to ultrasonic exposure.

2.5.3 Irradiation Procedure

Sites are irradiated in alternate cerebral hemispheres to allow ample time for any induced temperature gradients to dissipate and to allow any alteration of local blood flow to renormalize, before the next adjacent site is irradiated. When numerous sites (up to 16) are to be exposed in a single specimen, alternation of anterior and posterior sites is also employed. Body and brain temperatures are recorded along with the ultrasonic irradiation parameters and geometric locations for each exposure.

2.5.4 Site Selection

Sites are chosen with the aid of the stereotaxic altas of Jasper and Ajmone-Marson (1960). Specific sites are identified by the nature of the experimental objective, homogeniety of tissue type, size of the structures to be exposed, distance from ventricles, depth in the brain, and with regard to the number of sites to be exposed. For example, long-time exposures in superior brain structures often cause wide-spread destruction by heat conduction in adjacent tissue which is less vascularized as in white matter brain tissue. Under such exposure conditions, selected sites must be well within gray matter areas. Also, heat conduction along fiber tracts and tissue degeneration along these tracts leads to more widely dispersed lesion development (Fry, 1958) which requires ample spacing between sites in fiber tracts. Additionally, exposures made below a large ventricle are incorrectly compensated in intensity by the intensity depth correction described above, since a significant portion of the path length would be in low

attenuation cerebrospinal fluid. Therefore, lesion threshold sites should be placed above large ventricles to ensure correct delivered intensity. Brain coordinates for selected sites are then added or subtracted from the fiduciary zero coordinates of the calibrated irradiation platform to establish irradiation positions in the brain during the exposure. Sites typically chosen are in the area of the lateral geniculate, superior colliculus, substantia reticularis mesencephalica, lateral hypothalamus, caudate nucleus, and the region of the globus pallidus.

2.5.6 Post-irradiation Procedure

After exposure, the head pan is drained and removed. The wound is closed by surgically approximating the temporalis muscle right to left with sutures and closing the incision with interrupted sutures or wound clips, leaving a drain opening. The animal is removed from the stereotaxic frame and kept warm during recovery for 24 hours in a padded surgical recovery cage.

At 24 hours post-irradiation, the animal is injected i.p. at twice the original anesthetic dose of sodium pentabarbitol to ensure rapid and deep anesthesia. The animal is positioned with the ventral side superior on a horizontal autopsy frame and the extremities are extended and affixed to the frame. A mid-line, ventral incision is made from mid-thorax to lower abdomen. The xiphoid process is located and tissue is dissected away while elevating the cartilage. Entry into the thoracic cavity is made under the xiphoid to minimize bleeding. After the muscular and tendon attachments to the xiphoid are cleared, pneumothorax will occur and an opening sufficient for rib cutters will be obtained. The chest is opened by cutting along the mid-line of the sternum to mid-thorax. The ribs are spread apart and maintained in this open position with rib-spreaders to facilitate operating within the chest cavity. The heart is freed of its pleural

attachments and pericardial fat is excised. The pericardial sac is incised at the apex of the heart and then cut from the apex to the area of the high aorta with tissue scissors. The aorta is dissected from adjacent structures and a ligature is passed under the aorta and a lose, first tie is made to secure subsequent cannulation. The left ventricle is opened near the apex and a cannula inserted, passed through the mitral valve high into the aorta, and secured by the ligature. Perfusion is started with 900 ml of physiological saline pH 7.1 $\pm$ 0.1. The right atrium can be opened to speed the flow. Less than two minutes should be required for the 900 ml to perfuse, in a typical preparation. Without interruption, the 900 ml of saline is followed by one hour continuous perfusion with 10% formalin in physiological saline. Visual examination of other organs is performed during this period, in order to assess the state of health of the animal. Any abnormalities, such as intra-peritoneal fluid contamination, liver discoloration, gallbladder or speen enlargement, or developmental abnormalities are noted on the sacrifice data sheets. After one hour of perfusion with 10% formalin in physiological saline, perfusion is stopped, the head is removed, and the brain is dissected free. The brain is stored in the 10% formalin perfusion solution.

2.6 Tissue Examination

2.6.1 Histological Preparation

In preparing the tissue for embedding, a pin is inserted in the left side of the brain parallel to the midline to eliminate mounting errors. The brain is washed in distilled water and then dehydrated by immersion in increasing concentrations of ethanol. The organ is then cleared in methyl benzoate and imbedded in paraffin after which serial coronal, whole brain sections are made at 10 µm. Every tenth section is mounted for staining, with other sections saved in case

further histological procedures are required.

Differential stains for the demonstration of phospholipds, especially myelin, are used, viz., Luxol fast blue stain, (Thompson, 1966), cresylecht violet counter stain, and Wiel's myelin stain (Lillie, 1954), have been employed.

2.6.2 Slide Examination

The approximately 225 to 300 slides per brain are initially scanned to locate the slide where the griseum centrale appears to divide in the region of the nucleous habenularis medialis and to locate the slide where the optic chiasma first appears. According to the stereotoxic altas, these landmarks occur at frontal planes 7.25 and 13.25, respectively. The ratio of the difference in slide numbers to the difference in the atlas coordinates determines a scaling factor of each brain specimen after histological preparation. This scaling factor varies from animal to animal due to slight differences in brain size and to the variations introduced by dehydration and rehydration before the mounting of the sections. The ratio is then used to determine the slide number where the irradiation site should appear, given the known atlas coordinates. (It must be remembered that the vertical zero coordinate of most atlases is 1 cm above the "ear-bar zero" line of the animal.)

Additional landmarks are taken for the appearance of the anterior and posterior sections of the mamillary bodies at frontal planes 9.5 and 8.0. These deep brain landmarks, combined with the more superior landmarks taken previously, are used to determine the vertical angle at which the brain was sectioned. Since the brain is sectioned at very nearly a vertical angle (within $\pm 2^{o}$), subsequent data correction due to noncoincidence of histological geometry with irradiation geometry is not needed. That is, the vertical plane through any lesion to be measured is parallel to the major axis of the lesion. The coplanar geometry

facilitates the calculation of lesion volumes.

The slides for a particular lesion site are assembled and the slide containing the maximum lesion dimensions is chosen for measurement. The major and minor axes are measured with a transparent comparator scale under magnification, with the smallest division on the scale being 0.1 mm. The major source of error occurs due to the subjective determination of the exact location of the lesion boundaries. The periphery of some lesions show diffuse areas of thermal damage due to heat diffusion away from the central area (Fry, 1958). This causes slight changes in the myelin in the area and slight changes in the depth of histological staining. The degree to which this occurs is dependent, to some extent, on the irradiation parameters and to a greater extent on the staining procedure selected. The typical error in the linear measurement of the lesions was found to be $\pm$0.1 mm and this has been verified by the remeasurement of randomly selected lesions.

There were two types of experiments conducted which used the experimental techniques described. The first was a lesion volume study to correlate exposure parameters with the observed magnitude of the produced lesion size. The second study conducted was the determination of the level of the irradiation intensity and time duration of exposure for the appearance of a lesion at a previously unexamined frequency of 7 MHz. This is a threshold phenomenon and the determination of the threshold level is described below.

2.7 Threshold Level Determination

For those animals which were irradiated to determine threshold levels, slides are examined for the presence or absence of lesions at the irradiated sites. Where lesions have occurred at very near threshold levels, confusion may arise due to the presence of other histological entities of similar size, shape, and appearance. If further examination under higher power magnification fails to show clear

evidence of cell degeneration, it may be necessary to stain adjacent tissue sections $\pm 10\,\mu$. The use of different histological dyes often resolves borderline cases where cell structure remains intact but where evidence of beginning degeneration occurs such as, demyelination, swelling of nerve cell bodies and disintegration of glial cells.

To determine the threshold level, the square-root of the product of the highest intensity at a fixed exposure time, which does not produce a lesion, times the lowest intensity, which does produce a lesion, is taken (Dunn et al., 1975). Conversely, the intensity may be held fixed and irradiation durations may be varied to find the threshold exposure time. The threshold level is then refined by subsequent animal irradiations at levels much closer to previously determined threshold intensities and times.

2.8 Lesion Volume Study

For the portion of the study undertaken to correlate absorbed dose, dose rate, and lesion volume, lesions were selected which were well formed and wholly within a site of a single tissue type, i.e., white or gray matter. A well-formed lesion is defined as one in which the cross-sectional shape is very nearly spherical or ellipsoidal with well defined and continuous boundaries exhibiting no evidence of distortion due to hemorrhagic involvement or tissue mechanical failure due to structural weakness or any evidence of cavitation having been present. Lesions greater than 100 mm^3 tend to show signs of hemorrhagic enlargement. Thus, an upper limit of about 100 mm^3 was imposed for this study. Histological structures on the order of 0.01 mm^3 set a lower limit on the detectability of small lesions in the background of numerous histological entities of similar size and appearance.

Lesions may also be altered by heat flow along fiber tracts. Lesions near

fiber tracts or in areas which open into ventricular spaces are similarly excluded due to anamalous behavior caused by extraneous physiological influences on lesion formation (Fry, 1958).

During the course of the data aquisition, it was noted that inter-animal variations occurred in lesion volumes for ostensibly indentical irradiation parameters, i.e., lesion volumes varied as much as 25%. Though a portion of this variation can be attributed to the histological tissue processing, a significant portion of these differences may now be ascribed to variation in the delivered acoustic intensity due to the effects resulting from the presence of the brain meninges, which will be discussed in detail. In order to lessen inter-animal differences for data taken at various intensities, animals were subsequently irradiated at multiple intensities instead of fixed intensities. These multiple levels and times produced better correlations between dose and effect (Johnston and Dunn, 1976). Dose is approximated here as the product of the intensity (I) delivered to the site, times the intensity absorption coefficient (μ) of the tissue, and the duration of the exposure (t). This product (μIt) is then a first order approximation of the total energy absorbed per unit volume by the tissue at the focus of the transducer. Later work has shown an additional correction is needed for the frequency dependent attenuation of the delivered intensity due to the brain meninges. This introduces a constant factor by which the previously obtained results can be multiplied for the 4 MHz and 3 MHz data. This correction has little effect on the relative relationship between the results at the two frequencies and serves mainly better to establish absolute levels of energy absorbed.

Chapter 3

RESULTS OF LESION VOLUME STUDY

In order to investigate the dose-effect relationship between absorbed energy per unit volume and observed lesion dimensions, a series of animals were irradiated, as described in Chapter 2, at a wide range of exposure dosages to establish a graded series of lesion volumes.

A total of 25 animals were irradiated for the lesion volume study; ten at 4 MHz and 15 at 3 MHz. Six to eight lesions per animal were produced, depending upon lesion size and tissue space constraints. Of these, 140 lesions were measured on the slides which exhibited the maxima of linear lesion dimensions. The following data were recorded for each measured lesion: cat number, slide number, lesion length, lesion width, irradiation intensity, duration, irradiation frequency, and any additional remarks concerning tissue type irradiated (gray or white matter) or any anamolous behavior observed. Lesion placement was confirmed by observing lesion depth below the brain surface and lateral distance from the brain mid-line in order to correlate irradiation parameters with observed histological results and to verify the previously made depth corrections on the delivered intensity due to path length attenuation. In order to obtain a measure of the degree to which reproducible size results could be realized for the estimation of lesion linear dimensions, eight animals were selected randomly for reexamination. Forty lesions were remeasured and compared with the previously measured results with the maximum error in any lesion dimension measurements being $\pm$0.1 mm.

3.1 Data Analysis

Analysis of the data was aided by computer computation. The data were grouped by frequency and then by delivered intensity. The groups were then analyzed by calculating a first approximation of the lesion volume. It was assumed that the lesions were very nearly ellipsoids with circular cross-section (prolate spheriods). This is an acceptable approximation for setereotaxic focal lesions where the coincidence of the histological tissue sectioning process and irradiation stereotaxic geometry can be closely controlled. Hence, all brain sections measured on the microscope slides are closely parallel to the major axis of the lesion, and thus, the measurement of height and width on the slide with the maximum linear lesion dimensions constitutes an accurate measure of the major and minor axes of the ellipsoid. The volume is then,

$$V = 4/3\pi\ ab^2, \tag{3-1}$$

where, a, is the semi-major axis or one-half the height, and, b is the semi-minor axis or one-half of the width. Results obtained by this method are equivalent to those obtained by using Simpson's Rule for the integration of irregular areas (Hodgman, 1954).

A computer program was written which correlates, at each intensity, the volumes and irradiation times by doing a linear regression for the logarithm of the volume versus the logarithm of the time. A standard deviation of both the slope and intercept is also calculated as an indication of the relative correlation of lesion volume and irradiation times for each intensity.

The eccentricity of each ellipsoid was also calculated in order to compute the surface area of each lesion. It was hypothesized that it might have been possible to correlate the energy absorbed in the lesion volume with the thermal flux through the surface area of the lesion boundary. However, there were

insufficient data points to obtain good statistical correlations between exposure times and surface areas due to the scatter in the calculated areas.

3.2 Lesion Volume Results

Figure 3-1 shows the lesion volumes for various intensities at 4 MHz as a function of irradiation duration. The error bars exhibit the maximum uncertainty in the volume due to linear measurement errors. The maximum error occurs at small lesion volumes where the $\pm$0.1 mm uncertainty is a significant proportion of the total dimension. The slope of the lines increase with increasing intensity, except for the 150 W/cm^2 curve being a possible exception, at 150 W/cm^2 the slope is 2.8, decreasing to 1.8 at 300 W/cm^2, and then increasing to 2.0 at 750 W/cm^2, and to 2.2 at 2500 W/cm^2. The results displayed in this plot show the graded tissue response of observed lesion volume as a function of the duration of the applied irradiation and offer a basis for the development of a dose-effect relationship.

If it is assumed that only that portion of the ultrasound which is absorbed in the region of the focus of the beam by the tissue during the time of the irradiation can affect the state of the tissue, the energy absorbed is chosen as the dosimetric quantity. The intensity absorption coefficient (μ), times the intensity (I) gives the rate of energy absorption per unit volume per unit time. When this is multiplied by the duration of the exposure (t) in seconds, the energy per unit volume absorbed by the tissue in the region of the focus of the beam is obtained (μIt).

Some assumptions are required to obtain experimental verification of the approximation for absorbed energy per unit volume and its relations to produced lesion volume. First, the sound field distribution within the lesion volume may be considered uniform. Consideration of the wavelengths employed (approximately

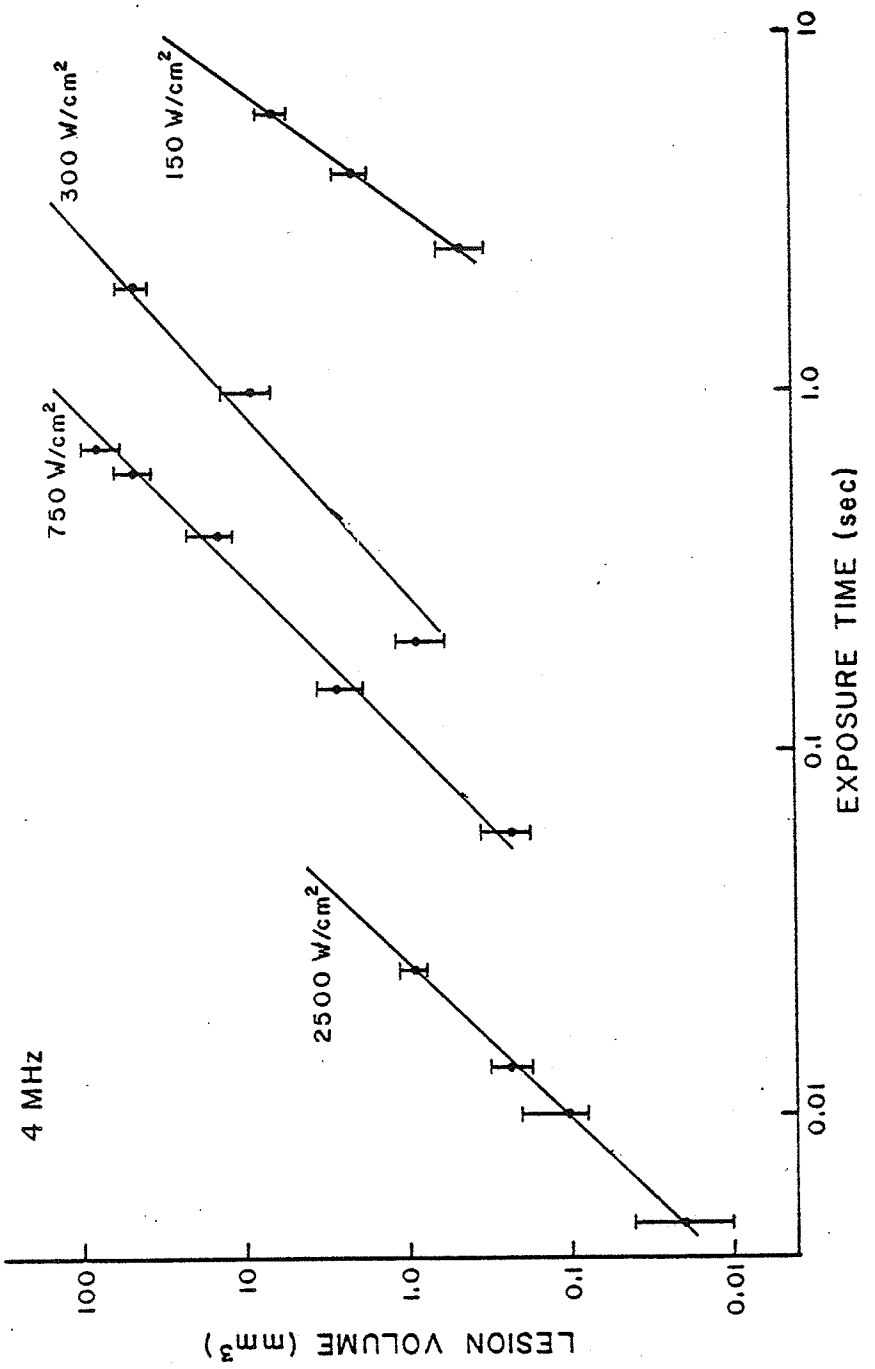

FIGURE 3-1 Lesion volume *versus* exposure time, with acoustic intensity being the parameter from curve to curve. Each point determined by five measured lesions.

0.4 mm), the linear dimensions dealt with in the lesion volumes (0.2 to 4 mm), and the geometry of the focused ultrasonic field (approximately 1λ) suggests that the errors introduced are less than the uncertainties associated with the linear measurements. Second, it is assumed that the ultrasonic absorption coefficient of the tissue was constant during the period of the exposure though this may not always be true (Dunn and Brady, 1973, 1974). However, the relatively short path of sound through the focal volume--the only portion of the path wherein significantly high intensity values are developed--determines that even the suggested tripling (Dunn and Brady, 1973, 1974) of the absorption coefficient would not alter the intensity over the path length in the focus and contribute errors as great as those of the microscopic linear measurements. With these conditions, data, and previous methods (Fry et al., 1970; Dunn et al., 1975) the ultrasonic intensity delivered to the lesion site and the ultrasonic energy absorbed therein where determined.

Figure 3-2 shows a plot of the lesion volume as a function of the absorbed energy per unit volume of lesion and delivered intensity at 4 MHz. Here again it is shown that the dose-effect relationship which exists between delivered acoustic dose and the observed effect of lesion volume is monotonic. This graph also shows that there is an additional factor to be considered in this dose-effect response, that is, dose rate or intensity. Not only does the lesion volume produced depend upon the total energy absorbed at the focus, but also on the rate at which that energy is delivered. Also, to produce a lesion of a given volume, less energy per unit volume is required at higher dose rates (higher intensities), for the range considered in this study. At intensities above 2500 W/cm^2, discontinuities in the mechanical response of the tissue such as cavitation may require modifications to the above dosimetric considerations. At very

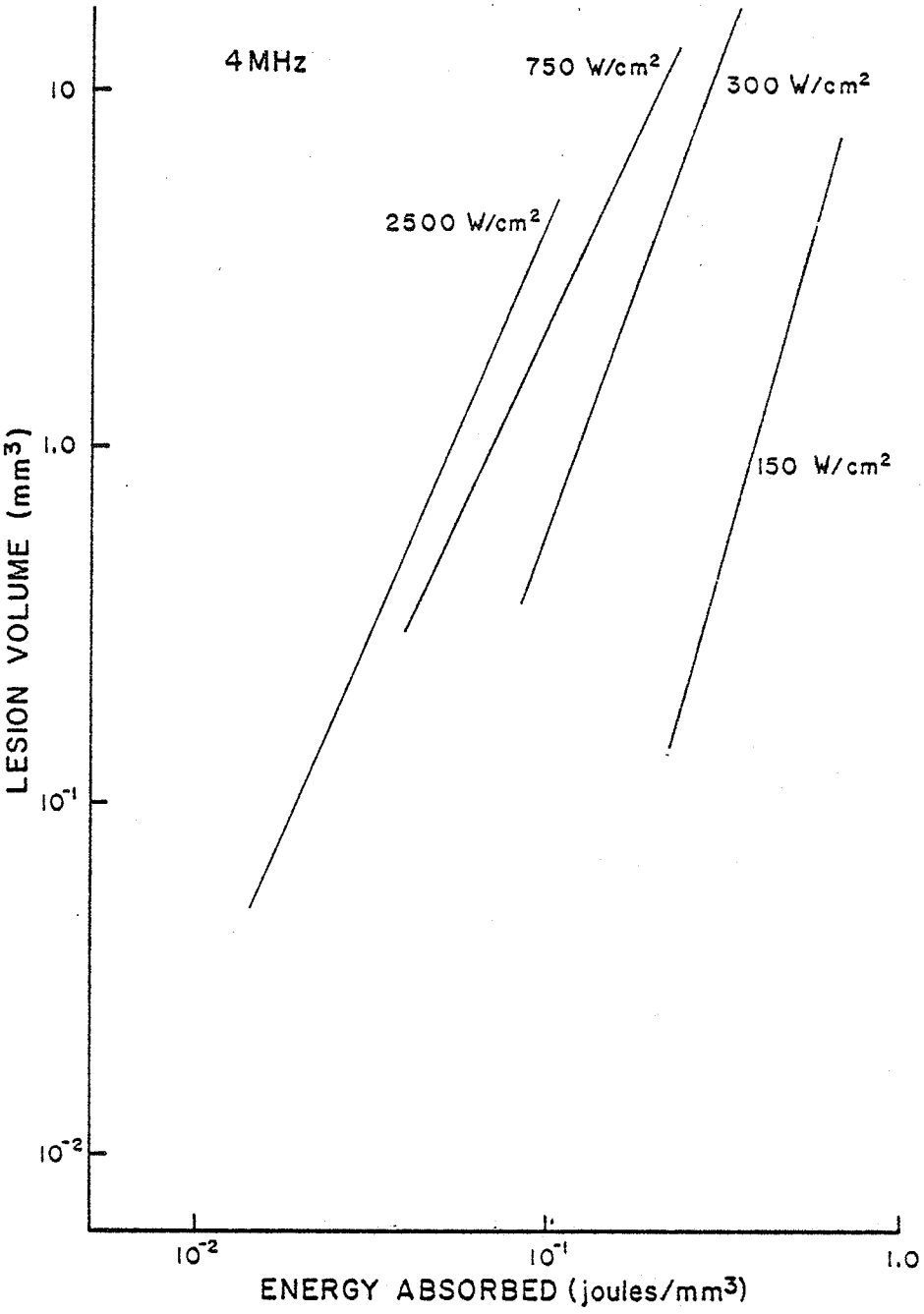

FIGURE 3-2 Lesion volume *versus* energy absorbed per unit volume

low intensities, viz., less than 100 W/cm^2, thermal conduction and physiological reactions to hyperthermia may also involve additional considerations.

If dose rate is a prime consideration in the development of a dosimetric quantity, it is useful to replot the above data as a function of intensity and Figure 3-3 shows the absorbed ultrasonic energy per unit volume as a function of delivered intensity at 4 MHz. The straight line is the threshold for lesion production (Dunn et al., 1975). The curved lines above the threshold are isovolumetric curves for lesions of 0.1, 1.0, and 10 mm^3, respectively. The dashed lines represent the curve for 0.1 mm^3 in the region near threshold where no data points were obtained. Figure 3-4 is a similar plot for the data available at 3 MHz, wherein the dashed lines represent estimated behavior at 10 mm^3 and 0.1 mm^3 where few data points were obtainable at the low intensities.

The results of irradiations at 3 and 4 MHz are combined in Figure 3-5 showing the absorbed ultrasonic energy per unit volume as a function of delivered intensity. Again, the straight lines represent threshold levels of 3 and 4 MHz. The lesion volume results for 3 and 4 MHz overlap well even within those regions where experimental errors are small. For example, results for lesions of volumes 1.0 mm^3 and above, and results for lesions produced at high intensities and short durations, correspondwell for 3 and 4 MHz.

Presenting the data in this format shows that for the supra-threshold effect of increasing lesion volume, as a function of delivered acoustic dose, can be described in terms of the product of the tissue intensity absorption coefficient, the intensity, and the irradiation duration. This is shown over two orders of magnitude in the observed effect of lesion volume, two orders of magnitude in delivered intensities, and four orders of magnitude in time duration of exposures. The frequency dependent variation in the tissue intensity absorption coefficient

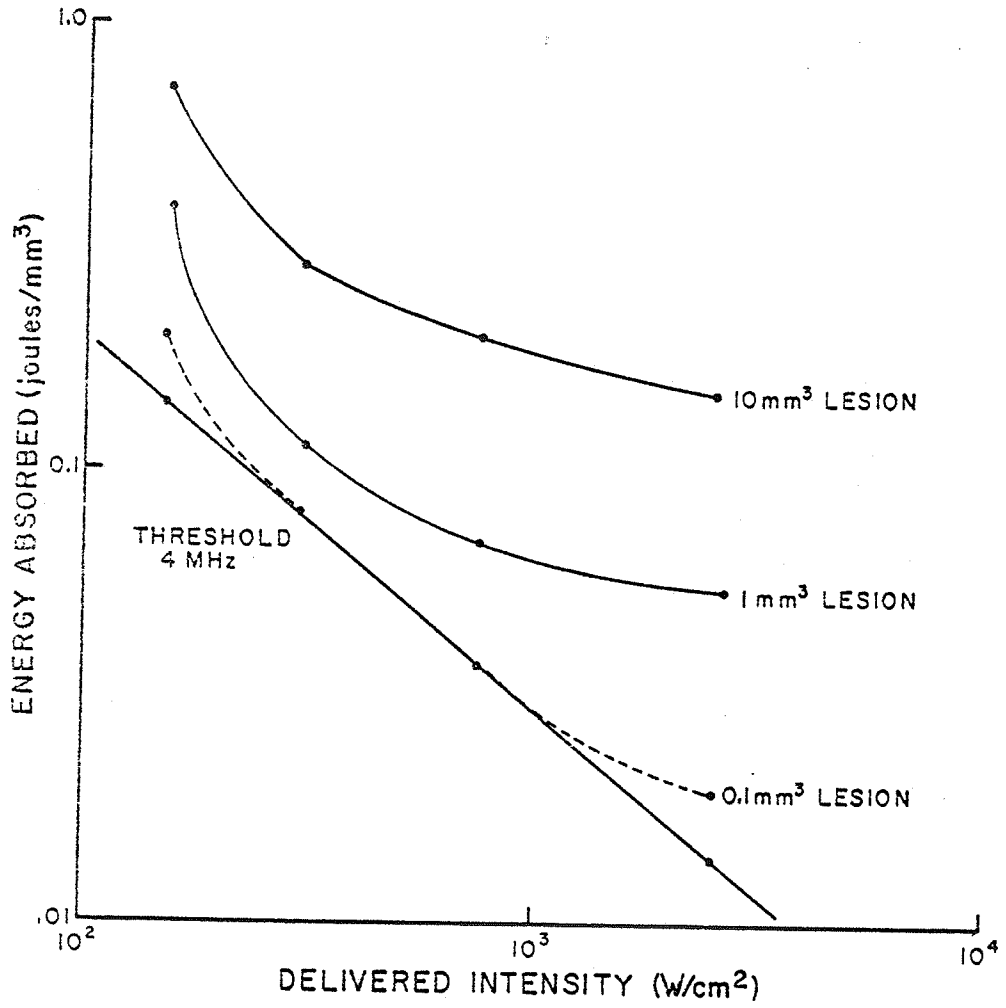

FIGURE 3-3 Energy absorbed per unit volume *versus* delivered intensity at 4 MHz, curved lines indicate isovolumetric lines for lesions volumes and straight line indicates threshold.

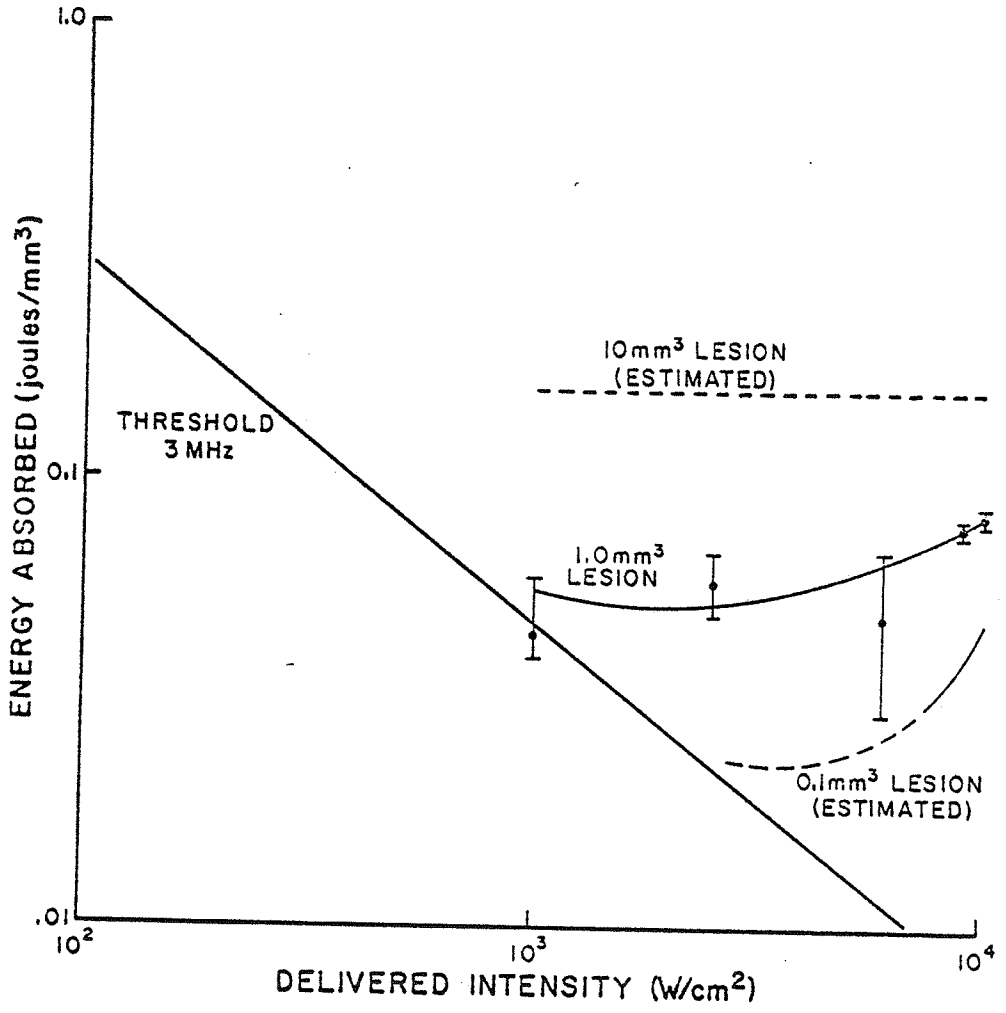

FIGURE 3-4 Energy absorbed per unit volume *versus* delivered intensity at 3 MHz showing isovolumetric lines and straight line of threshold.

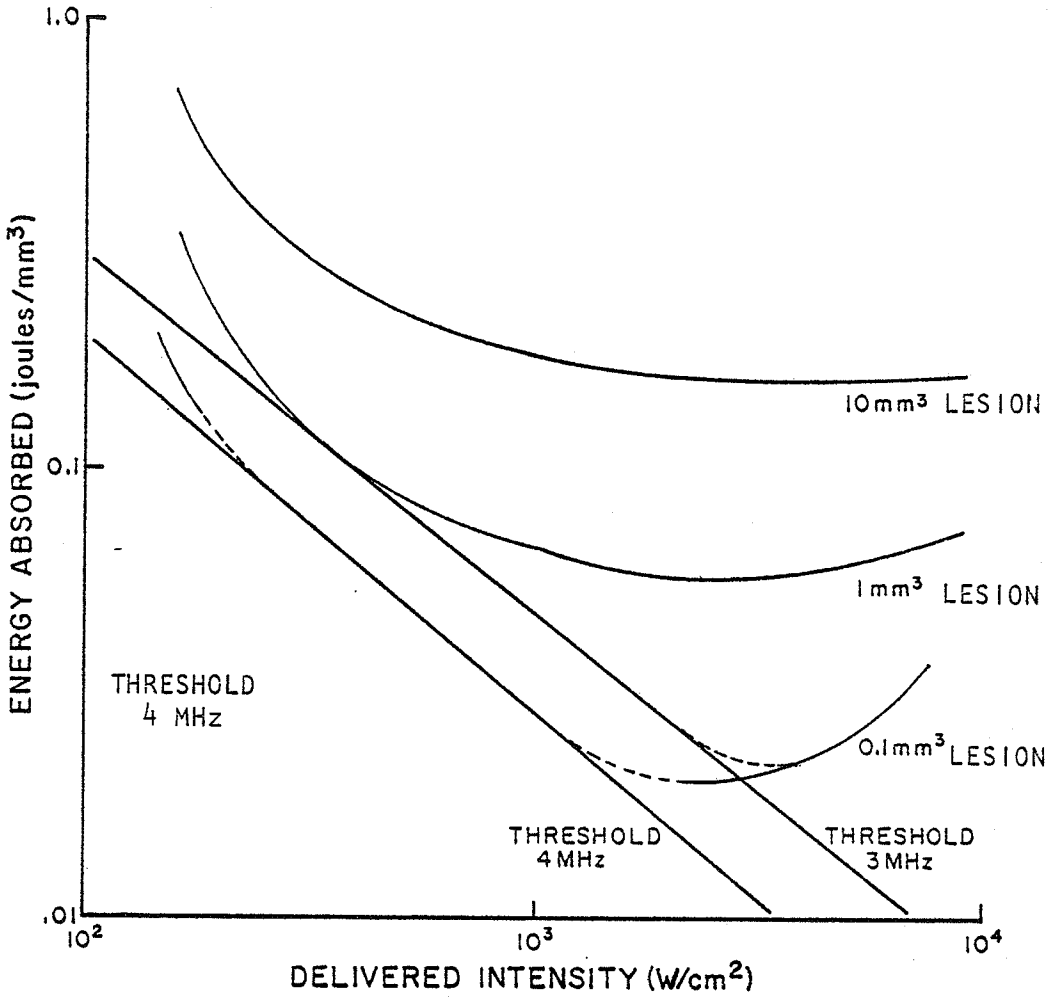

FIGURE 3-5 Combined results of 3 and 4 MHz energy absorbed per unit volume *versus* delivered intensity. Curved lines indicate isovolumertric lines for lesion volumes and straight-lines indicate lesion thresholds at 3 and 4 MHz.

and its contribution to the absorbed dose are here checked only at two frequencies. Animals which were irradiated at 1 and 9 MHz for other experiments in this laboratory were found to be unsuitable for this work since each animal was irradiated only at fixed intensities in an effort to establish threshold times. It would require irradiation at multiple intensities and times within each animal to eliminate variabilities as were described previously in the experimental methods section.

The combined results of irradiations at 3 and 4 MHz for both white and gray matter of the brain show good agreement and implicate absorbed energy per unit volume as a good dosimetric parameter when data is plotted as a function of dose rate. It is interesting to speculate that these results suggest that a similar set of curves exist, for the energy absorbed per unit volume *versus* the delivered intensity, for other tissues as well. Note that slight differences in thresholds, as a function of frequency, will produce some differences in any such set of curves.

Chapter 4

EFFECTS ON OBSERVED LESION THRESHOLDS DUE TO ANATOMICAL STRUCTURE

As good correlations between the supra-threshold effect of increasing lesion volume with increasing absorbed dose were observed, the question is raised why the threshold levels of absorbed energy were so different at each frequency. Additionally, as frequency increases neither does the absorbed dose nor does the intensity level for threshold behavior increase monotonically. Figure 4-1 shows the delivered acoustic intensity required to produce a threshold lesion as a function of the duration of exposure for 1, 3, 4, 4.5, and 9 MHz for a total of 62 animals and 684 irradiations as reported by Dunn et al. (1975). Each line is describable by the relation in which the product of the intensity times the square-root of the exposure duration equals a constant which depends on the frequency. In order to determine this constant and a statistical range, the mean slope of the line for each frequency in Figure 4-1 was determined along with the standard deviation times a confidence factor inversely proportional to the number of data points. The confidence factor is the student t factor $t_{.5(N)}$ for N degrees of freedom and P = 0.95, where N equals the number of data points, used to calculate each slope, minus 2. Using the mean of the slope and the standard deviation times t, the intercept of each line in Figure 4-1 at 1 second (where log t = 0) was evaluated and a range above and below this threshold intercept constant was determined.

Figure 4-2 shows the values of this constant as a function of the irradiation frequency. Alternatively, the values of intensity displayed in Figure 4-2 are the threshold intensity levels in Watt per square centermeter required to produce a

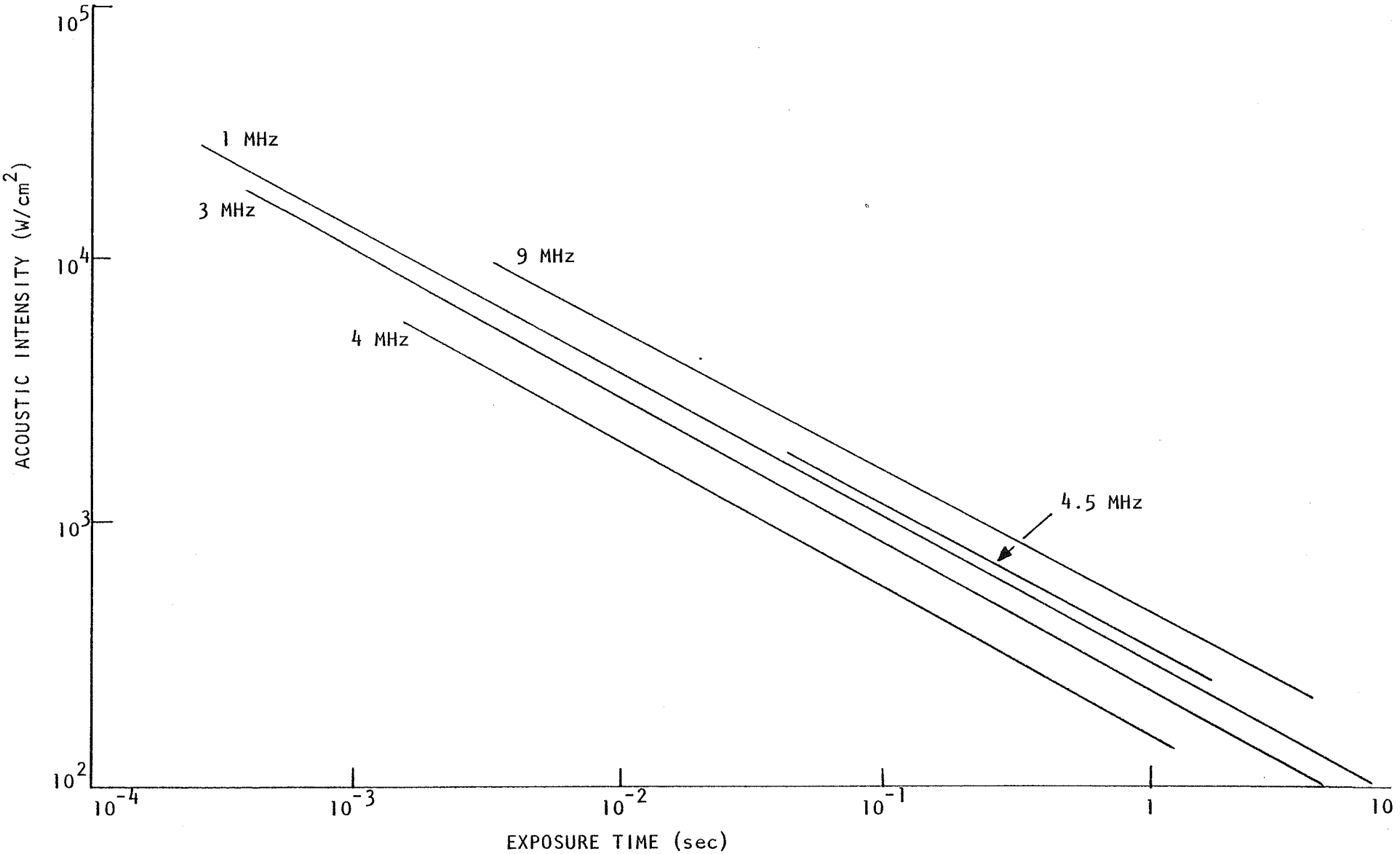

FIGURE 4-1 (from Dunn et al., 1975) Acoustic intensity *versus* exposure time required to produce a brain lesion at threshold for the irradiation frequencies indicated.

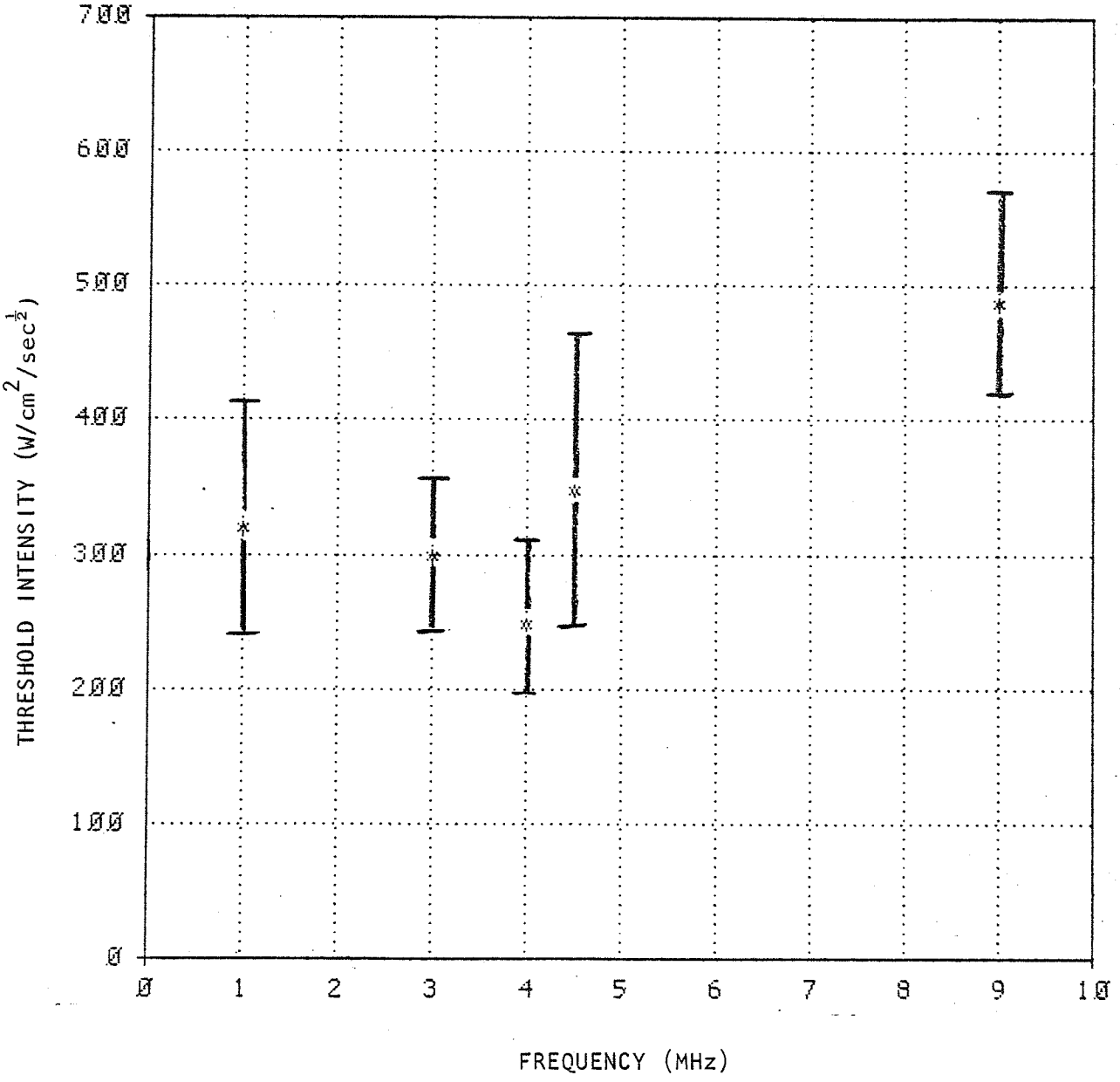

FIGURE 4-2 Threshold intensity *versus* frequency

lesion at a 1 second exposure, shown as a function of frequency. Threshold intensity values appear to decrease from 1 MHz to 4 MHz and then increase from 4 MHz up to 9 MHz.

4.1 Brain Anatomical Considerations

Certain brain anatomical structures which are unique to this organ may be giving rise to acoustical inhomogeneities in density and sound velocity. All organs of the body are encapsulated by a tough collagenous membrane which serves in a structural maintenance and supporting role. The brain has additional layers of membranous protection plus a fibrous mesh of supporting collagen filaments between layers.

The central nervous system is enclosed by three membranes as shown for the brain in Figure 4-3, a partial coronal section near the surface; the dura mater, the arachnoid, and the pia mater which is closely adherent to the surface topology of the brain and spinal cord. The outer membrane, the dura mater, is a tough collagenous structure, but with very little acoustic attenuation as has been shown by *in vitro* measurements (Basauri and Lele, 1962). This layer closely overlies the second meningeal layer, the thin arachnoid membrane. This delicate layer encloses the subarachnoid space which contains cerebrospinal fluid and the web-like structure of connective collagen fibers (Lockhard et al., 1972) which extend between the arachnoid above the third membranous layer, and the pia mater, below (Ranson and Clark, 1959).

It is hypothesized that the structure responsible for the frequency dependent variations in threshold lesion levels is the sub-arachnoid space and the network of collagen fibers, the sub-arachnoid trabeculae, which lie in between. The very high, low-frequency bulk modulus of elasticity (Fields and Dunn, 1973) of the collagen fibers is considered to give rise to a stratum differing in acoustic

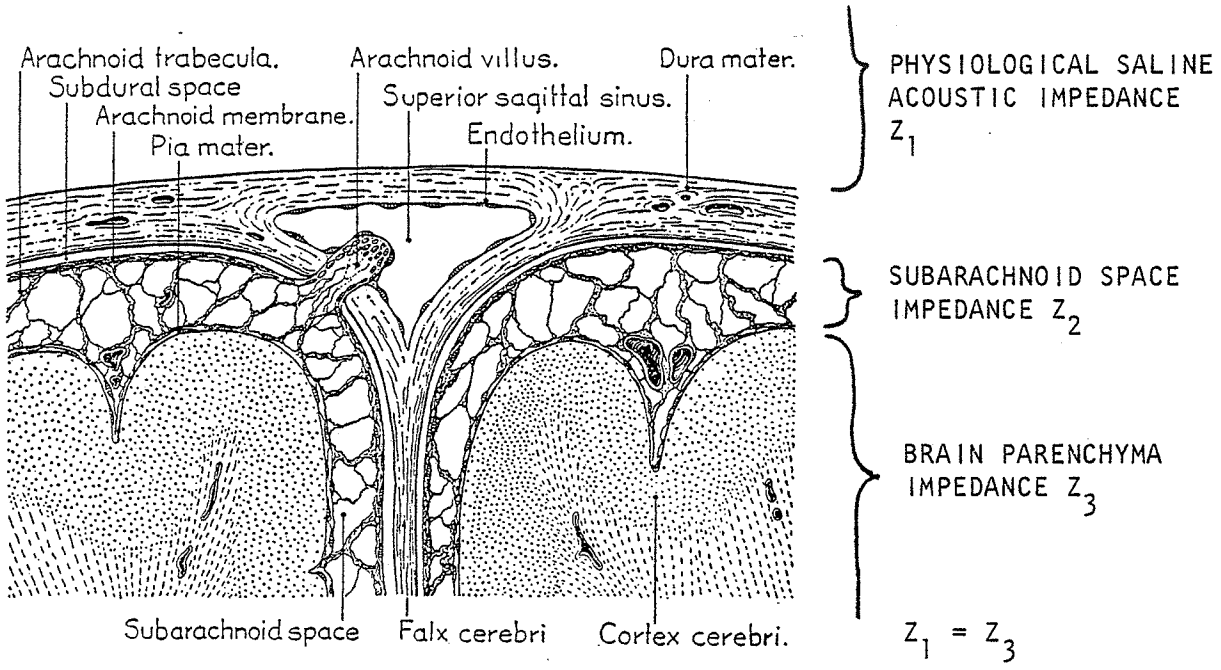

FIGURE 4-3. (After Ranson and Clark, 1959) Partial coronal section of the brain showing meningael structures and regions of differing acoustic impedance Z_1, Z_2, and Z_3.

impedance from that beyond the two bounding surfaces.

An additional factor which implicates the meningeal structures as the causative influence on the frequency variations in lesion threshold levels is seen when the dura is surgically removed. Stripping the dura, which is often attended by simultaneous disruption of the arachnoid integrity, can result in a five fold increase in observed lesion volumes as compared with similar irradiation of an intact animal (Basuari and Lele, 1962). The increased lesion volume is believed to result from the removal of some intensity attenuating structure, though attenuation measurements on the excised dura itself showed that only 5% of the incident intensity is attenuated by the dura (Basauri and Lele, 1962). This lends support to the view that the difference in observed lesion volume is due to the intact tissue and to the physical organization of tissue macrostructure beneath the dura mater.

Further evidence for the meningeal influence on thresholds is seen in ultrasound echographic scans of the brain. It is observed that the meningeal structures transmit only half of the incident intensity at some frequencies, which is caused by substantial reflection of incident energy due to a frequency dependent acoustic mismatch. Indeed, some of the strongest reflecting structures in the brain are those associated with the meninges (Kossoff, 1972). Signals returned from the superior brain meninges, falx cerebri (brain mid-line), and tentorium cerebelli are among the greatest in signal magnitude of any brain structures.

4.2 Mathematical Description

During irradiation, ultrasound is conducted from the focused transducer to the brain by a solution of physiological saline which has a characteristic acoustic impedance of Z_1 (Figure 4-3). The sound then passes through the dura,

arachnoid space, and pia membrane. Let the impedance of the sub-arachnoid region be denoted by Z_2 and let the brain parenchyma have an acoustic impedance of Z_3.

As an ultrasonic wave passes through each region, a certain portion is reflected at each impedance discontinuity. In the region of the sub-arachnoid space, a partial standing wave is created which acts on the Z_1--Z_2 interface to modify the transmission characteristics of that boundary. The effect of these plane and parallel contiguous layers on the transmitted wave intensity is well known for idealized media (Kinsler and Frey, 1962). In the present case, the physiological saline is very nearly equal to the impedance of the brain, i.e., it can be assumed that $Z_1 = Z_3$. The intensity transmission coefficient is then

$$\alpha_t = \frac{4}{4\cos^2(kl) + \left(\frac{Z_1}{Z_2} + \frac{Z_2}{Z_1}\right)\sin^2(kl)} \qquad (4\text{-}1)$$

where k is the wave number ($k = \frac{\omega}{c}$, where ω is the angular frequency and c is the velocity in the subarachnoid space), and l is the acoustic path length through the sub-arachnoid space. For this relationship to be valid, the sound waves must enter the brain at very nearly normal incidence and there must be no significant reflections from within the brain back to the sub-arachnoid structures. The first condition is met since the narrow beam width of the transducer (less than 30° half-angle) and the irradiation geometry ensure near normal incidence. The second condition is also met since the absorption and scattering of the ultrasound wave by the brain parenchyma would allow very little energy to be returned to the meningeal layers.

If the required tansmitted intensity to cause a lesion is I_t, it is possible

to calculate the necessary incident intensity (I_i) which would be required to be delivered in order to compensate for the attenuation of the brain meninges. If

$$\frac{I(\text{transmitted})}{I(\text{incident})} = \alpha_t, \tag{4-2}$$

Then

$$I_i = \frac{I_t}{\alpha_t} = I_t \left\{\cos^2 kl + \tfrac{1}{2}(Z_1/Z_2 + Z_2/Z_1)^2 \sin^2 kl \right\}, \tag{4-3}$$

from equation (4-1) with $Z_1 = Z_3$. Using the identity $\cos^2 kl + \sin^2 kl = 1$,

$$I_i = I_t(1 + A \sin^2 kl), \tag{4-4}$$

where

$$A = \tfrac{1}{4}(Z_1/Z_2 + Z_2/Z_1)^2 - 1. \tag{4-5}$$

In terms of the frequency (f),

$$I_i = I_t(1 + A \sin^2 \frac{2\pi f l}{c}), \tag{4-6}$$

where c is the sound velocity in the sub-arachnoid space, which may be largely due to the collagen fibers.

Figure 4-4 is a plot of the frequency dependence of the threshold intensity which shows the curve for equation (4-6) and the data points at 1, 3, 4, 4.5, and 9 MHz. By making suitable choices for the three constants in equation (4-6), a good fit can be made to the five experimentally determined values. The three constants are the required transmitted intensity (I_t), the combined impedance ratios (A, in equation (4-5)), and the ratio of l/c in the sine term. Since l, the average thickness of the sub-arachnoid space, is determined from anatomical

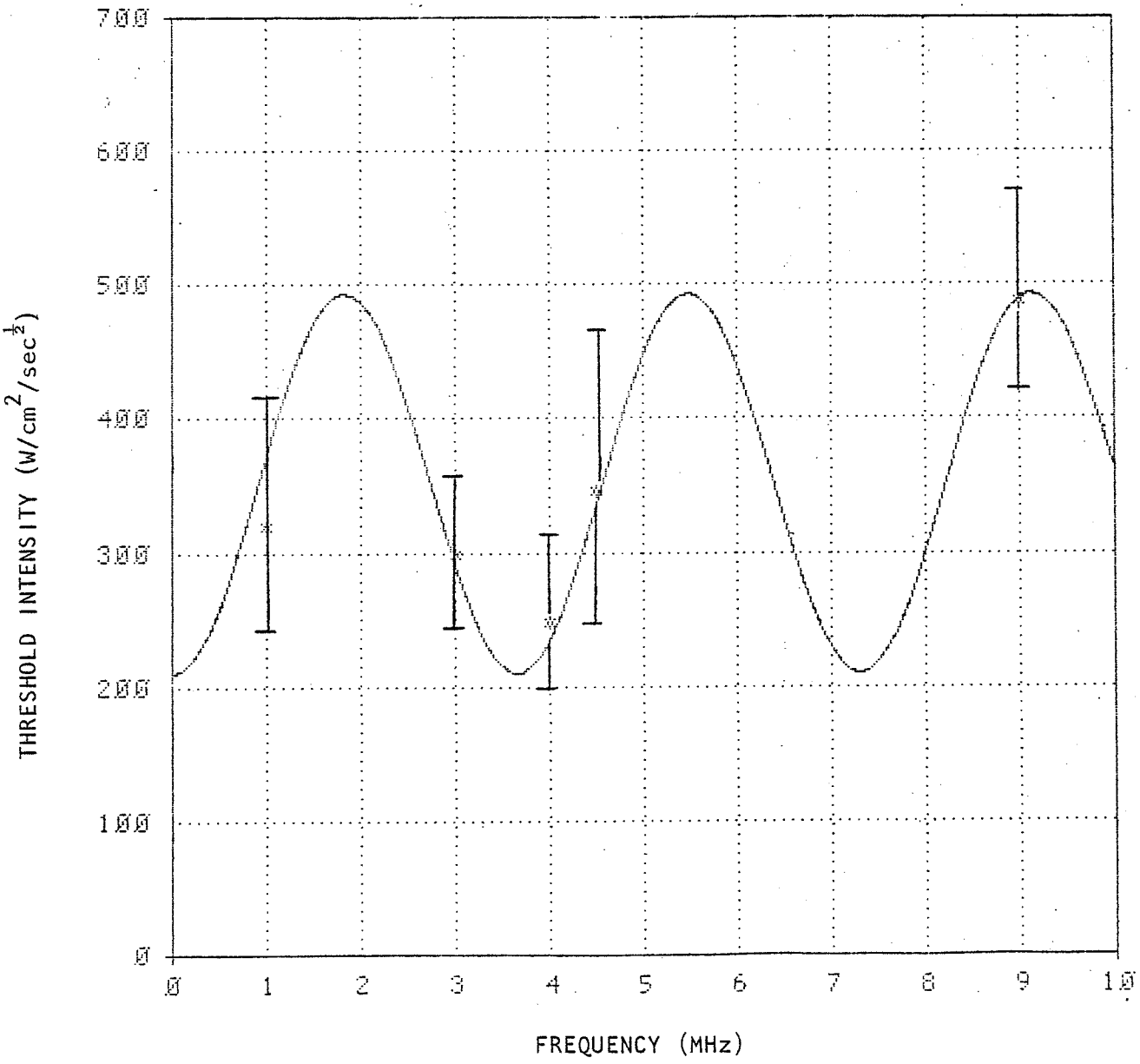

FIGURE 4-4 Threshold intensity *versus* frequency. Continuous line is the theoretical prediction of equation (4-6).

measurements (Weed, 1934) to be approximately 200-250 μm and since c, the sound velocity in the collagen fibers of the sub-arachnoid space, should have a value similar to other collagenous tissues, viz., 1600-2000 m/sec (Goss et al., 1978), the combined ratio of l/c is restricted by physical considerations. For equation (4-6), as shown in Figure 4-4, l was chosen to be 250 μm, c 1850 m/sec, A was 1.35, and I_t was chosen to be 210 W/cm^2.

4.3 7 MHz Threshold Determination

It is seen from Figure 4-4 that this theory predicts a series of minima and maxima in lesion threshold intensity with a minimum near 7 MHz. In order to test this theory, a series of irradiations were conducted at 7 MHz. The irradiation exposure intensity was held constant at 200 W/cm^2 and the exposure durations were varied to establish a threshold time. A total of eight animals were irradiated with eight exposure sites per animal and forty-six lesions were produced. Threshold levels were established for each animal by the technique described in Chapter 3. A broad range in the threshold intercept constant, the product of the intensity times the square-root of the exposure duration ($It^{\frac{1}{2}}$), was obtained, ranging from 206 W/cm^2/sec$^{\frac{1}{2}}$ to 125 W/cm^2/sec$^{\frac{1}{2}}$, with the mean value being 172 $\pm$ 46 W/cm^{2}sec$^{\frac{1}{2}}$ ($\pm$ one σ).

Figure 4-5 shows the point for the 7 MHz threshold determination with error bars at the P = 0.95 level ($\pm$ 2σ) combined with the experimental points previously obtained and the theoretical curve from equation (4-6). The mean threshold value falls below the predicted value by only 14%, and is well within the error bars.

Combining the 7 MHz threshold with the previous five threshold values and optimizing the fit of equation (4-6) by the method of least square error, modifies the values of the constants used in equation (4-6) by only a small amount. The value for l, the average thickness of the sub-arachnoid space is 250 μm. This

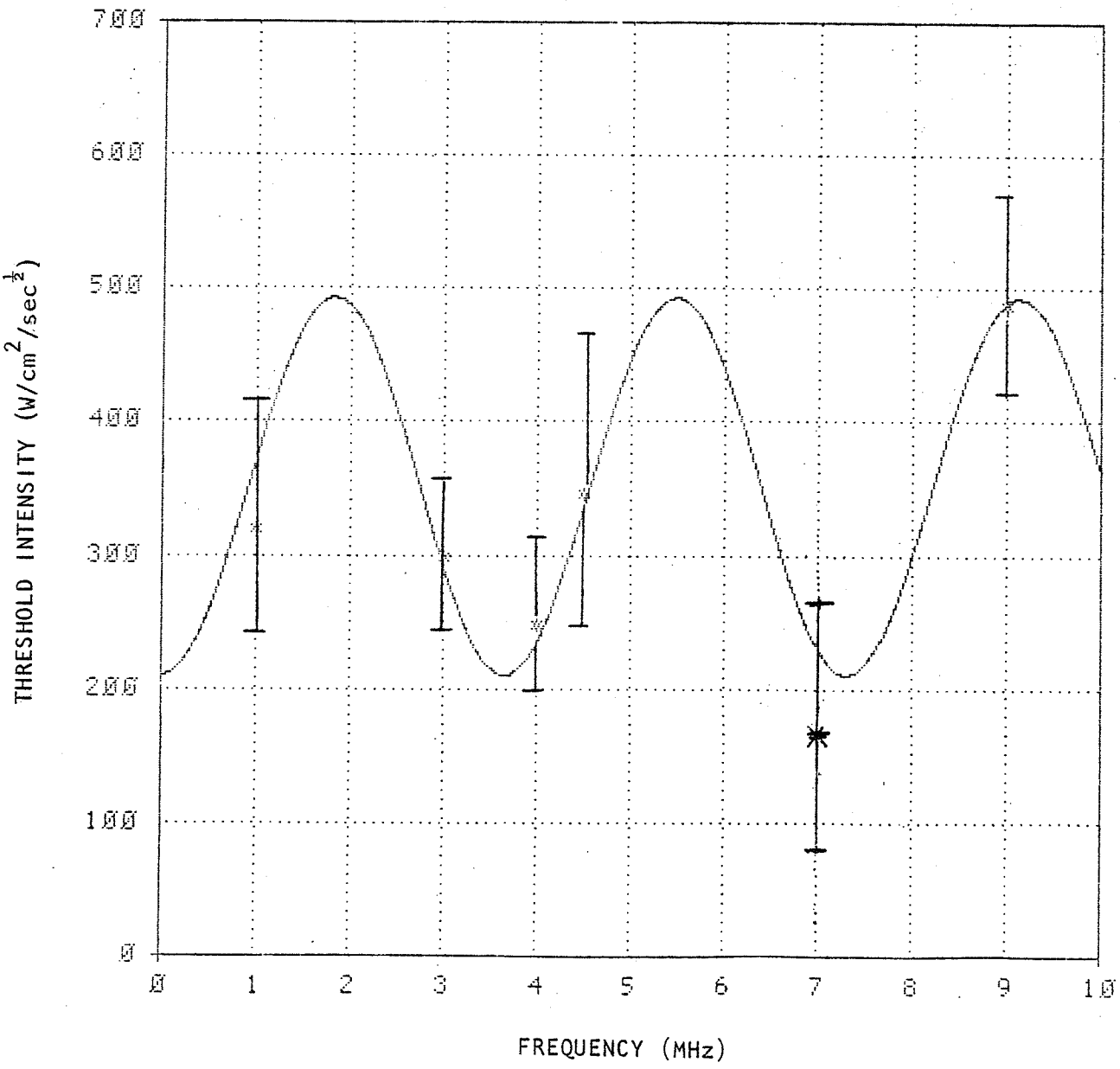

FIGURE 4-5 Intensity *versus* frequency showing additional point from the experimental threshold determination at 7 MHz and the continuous line indicating the theoretical prediction.

closely approximates literature values for cat brain (Weed, 1934) and represents the average value over the superior surface of the organ. In the regions of the sulci, the furrows of the brain, this value may increase by two or three fold. Since these regions constitute a small percentage of the total brain topography when compared with surface area above the gyri, the elevated convolutions of the brain, such localized variations can be ignored in the average anatomical dimensions.

The value for c of 1850 m/sec is consistent with the velocity measured in other collagenous tissues. Since the relative collagen content of the sub-arachnoid trabeculae has not been measured, only a general comparison with literature values can be made. Beef tendon which has a high collagen content (30%) was measured by Dussik and Fritch (1956) with a velocity of 1750 m/sec. Goss (1978) measured an average value of 1747 m/sec and a range of approximately 1700-1870 m/sec in mouse tail tendon perpendicular to the axis of the tendon thread.

The value of the constant A in equation (4-6) is a function of the impedance ratio of the sub-arachnoid space and the brain. The result of the least square error fit to the data yielded a value of A of 1.4 yielding a calculated acoustic impedance ratio of 2.3. Since the acoustic impedance is the product of the density and the sound velocity, comparison values may be calculated. For brain, the density is 1.028 gm/cm^3 and the velocity is 1550 m/sec (Robinson and Lele, 1972), which gives the impedance of 1.6×10^5 gm/cm^2-sec. For the sub-arachnoid fibers, a density in collagen of 1.33 gm/cm^3 (Holmes et al., 1977) may be used and the velocity of 1850 m/sec gives an acoustic impedance of 2.46×10^5 gm/cm^2-sec. The expected ratio is then 1.55 which is 28% less than predicted from equation (4-6). The difference between the two values may be considered to be due to the composite

nature of the sub-arachnoid space. Sound travels both in the solid-like phase collagen fibers and in the liquid-like phase cerbrospinal fluid. The difference in sound velocities is considered to give rise to a progressively increasing phase difference between the waves traveling in each mode. This tends to enhance slightly the apparent impedance effect of the sub-arachnoid fibers as calculated in equation (4-6) due to the interference when the two waves in each mode are summed at the pia mater interface.

The value of I_t, the intensity which must be delivered to the site in order to cause a lesion at 1 second exposure duration, was determined to be 200 W/cm^2. From this theory, it is a frequency independent threshold value for the brain parenchyma since it was assumed that the entire frequency dependent effecton the threshold, as observed by the value of the externally applied exposure intensity, was due to the acoustic impedance mismatch of the brain meninges. This independence of threshold intensity with frequency has been predicted for particular instances. Lerner et al. (1973) found that when heat alone is considered to be the cause of lesion production for exposure durations of 1 to 100 seconds, a mathematical model for heat generation at the focus was sufficient to explain observed threshold effects. It was noted in their analysis that the increase in absorption with frequency, combined with the decrease in focal volume, with increasing frequency, yielded a nearly frequency independent increment in the produced temperature at the focus.

4.4 Summary

The three layer model of the ultrasound tranmission characteristics of the brain meninges explains the previously observed frequency dependent variations in the apparent lesion threshold intensity and predicts the behavior at an untested frequency of 7 MHz. The theoretical fit to the six frequency data points

by suitable selection of three constants is not arbitrary or capricious. Firstly, it is mathematically sufficient since this procedure involves the solution of six simultaneous equations (equation (4-6) at each frequency) in only three unknowns (the constants of equation (4-6)). And secondly, the values of the constants correspond to physically realizable values which can be compared with independent sources.

The value of this result lies in its utility in normalization of observed exposure parameters as a function of frequency by correcting for tissue effects on the ultrasonic intensity delivered to the irradiation site. Such refinements of exposure values allows for a greater degree of confidence in defining dosimetric values. When external or exposure doses are well established, first approximations to absorbed doses can be made and possible modes of tissue interactions and mechanisms for observed bioeffects can be better postulated.

Chapter 5

MECHANISMS OF ULTRASOUND BIOLOGICAL EFFECTS

The physical mechanisms responsible for the observed biological effects of ultrasound associated with the high intensities employed in producing irreversible structural changes in mammalian brain tissue have been postulated to be of three main types depending upon the intensity at the site of interest and the duration of exposure (Pond, 1969; Robinson and Lele, 1971; Fry and Dunn, 1972). The thermal mechanism is involved at the relatively low intensities of less than several hundred Watts per square centimeter and for exposure durations greater than 1 second, and is concerened with the conversion of absorbed energy from the mechanical form to the thermal form. Mathematical models (Pond, 1969; Lerner et al., 1973) have been developed which reasonably correlate experimentally determined thresholds with the calculations. Additionally, Pond (1969) was able to mimic the thermal transients produced by focused ultrasound by the use of implanted electrically heated wires. The damage produced and the observed threshold behavior as determined by the heat energy involved, are sufficiently similar in all regards to give credence to the view that heat alone is sufficient to cause the observed effects.

A second mechanism of interaction of ultrasound and tissue is cavitation, the onset of which occurs after only short durations of exposures (milli-seconds) and for the high intensities employed herein, viz., $2 \times 10^3 - 2 \times 10^4$ W/cm^2. Here, clear histological evidence of the caprcious characteristics of this phenomenon exist (Pond, 1968; Fry et al., 1970) implicating cavitation as the primary

cause of tissue destruction. Ultrasonic cavitation occurs when high negative pressures causes cavities to be formed within the medium. When these inclusions collapse during high peak pressures, stored energy is released which causes the observed tissue damage.

Large lesions with irregular boundaries often occur at sites in the tissue which correspond to regions where tissue mechanical properties change abruptly, such as exist near blood vessel-parenchymal tissue boundaries. Lesions often occur at regions other than the expected (or anticipated) focal region of the soundbeam even though the intensity at the site is originally thought to be less than that at the focal region, indicating particular weakness in the mechanical strength of certain tissue structures, or identifying a site where cavitation nuclei may be more abundant. A nucleus for the initiation of a cavitation event in tissue may be a site where dissolved gasses are easily forced from solution under the high negative peak pressures produced by the high intensity ultrasound irradiation. Little is knownof the actual form of cavitation events in tissues. However, the gross mechanical disruption attending the presence of cavitation is clearly shown by torn tissue structures, hemorrhagic involvement, and blood-vessel disruption all of which are not seen in lesions of thermal origin (Fry et al., 1970). Pond (1968) and Gavrilov (1974) have shown that the temperature rise expected to be developed for these high intensities and short exposure durations, from involvement of only the thermal mechanism, would be less than a $5^{o}C$ rise at the focal region of the beam. This small temperature rise, coupled with the shortduration of its presence at the site can eliminate the thermal mechanism as responsible for the observed damage (Gavrilov, 1974).

A third interaction mechanism can be postulated to occur in the intermediate intensity region below the cavitation region and above the thermal region, viz.,

in the region 2,000 to 200 W/cm^2. Clearly cavitation can be ruled out in this region by histological examination of the irradiated tissue and by monitoring acoustically for evidence of the presence of cavitation, during exposure, by implanted acoustical sensors and by spectrum analysis of the observed signals, as wide-band acoustical signal of noise-like characteristics are evidence of transient cavitation (Esche, 1952; Neppiras, 1969). The thermal mode for lesion production may also be ruled out as calculations of temperature rise at these intermediate levels show that damaging temperature levels are not reached in the time the energy is present. Gavrilov (1974) calculated a temperature rise of only 4.5°C for 1000 W/cm^2 at 0.1 second at 3 MHz. Additional evidence for another mechanism to be operative in this intensity range and as being non-thermal in origin, has been provided by Fry et al. (1950) and Dunn (1958) who demonstrated that in neural tissue at least, an irreversible alteration of a functional endpoint is obtained in the absence of cavitation and without the temperature rising beyond 38°C, at which, damage can be induced by steady state application. Barnard et al. (1955) made similar observations in the brain tissue of cats at these intermediate intensities.

5.1 Non-thermal and Noncavitation Mechanisms of Ultrasound Bioeffects

A number of non-thermal non-cavitation mechanisms of interaction of ultrasound with biological matter which have been identified (Dunn and Pond, 1978; Nyborg, 1978) are considered to be sufficient to explain the observed ultrasound bioeffects. Nyborg cites the viscous stress exerted on a boundary, equal to the product of the velocity gradient and the shear viscosity. Such viscous stresses may be considered not only to exert forces on possible biological structures, but may also initiate other phenomena, such as acoustic streaming of intracellular contents or microstreaming of blood inside vessels which may ultimately comprise

the causative agent. These viscous stresses and hydrodynamically produced flows may cause biological effects which may irreversibly alter physiological functions of ultrasonically irradiated tissues. Dunn and Pond (1978) classify non-thermal ultrasound mechanical disarrangement of tissue structures into three main groups, viz., cyclic tissue effects, effects which sum over many cycles, and effects which are structure-shape dependent. Examples of cyclic tissue stresses are those forces produced by the bouyancy of structural inclusions which, by virture of density differences, undergo cyclic stresses due to the large acceleration experienced under the applied acoustic field. Time-averaged effects include radiation force due to the momentum of a traveling wave exerted on an absorbing medium or exerted at partially reflecting interfaces. Also included here are streaming effects and radiation torque due to the twisting action exerted on elements suspended in the fluid medium under effects of an applied acoustic field (Nyborg, 1978). The authors (Dunn and Pond, 1978) give details for each mechanism discussed and include numerical examples which indicate the possibility that these mechanims could occur in biological tissues and fluids under specific conditions. However, due to the complex nature of biological systems, clear evidence for the presence and action of these mechanisms can't always be demonstrated. For example, Gould and Coakley (1974) investigated the effects of radiation force on blood cells and found simple theory did not account for all observations. Thus, for sufficiently dilute solutions, the simple radiation force theory adequately described the observed effects. But at near physiological concentration levels, it appears that the theory must be modified completely to account for interparticle interactions and sufficient details allowing for accurate description of such events are lacking.

However, these mechanisms do not account for the results observed during lesion production in brain tissue at intensities in the range intermediate between the cavitation and thermal regions, and are cited to show that thermal lesion mechanisms below cavitation intensity levels do exist.

Other investigators (Lele and Pierce, 1972) argue that it is not necessary to invoke such non-thermal mechanisms to explain the observed behavior and that a "thermal hypothesis" may be extended by suitable models to describe such events. Their model is extended by considering intracellular differences in absorption and by postulating the existance of hypothetical "quasi-equilibrium states" through which the irradiated tissue elements must pass during irradiation. Lele and Pierce (1972) believe that by these modes of interaction, the thermal hypothesis may be extended to intensities where cavitation becomes the predominate mechanism of interaction. Lele (1977) also disagreed with the evidence for non-thermal effects as was shown by Fry et al. (1950) and Dunn (1958) wherein functional changes are produced at reduced temperatures and under conditions where the temperature rise results in acknowledged damaging temperature levels never being approached. Here, Lele (1977) believes that the rate of rise in temperature produced may be affecting the animals ability to make rapid metabolic accomodations to temperature, and leads to the observed irreversible functional alteration.

In what follows, the theory and mathematical development of a mode of ultrasound tissue interaction are described to account for tissue interaction in the intermediate intensity level range between the thermal and cavitation levels. It is felt that those who favor strictly mechanical mechanisms and those who favor a thermal hypothesis will find this mechanism acceptable and compatible with existing theories. It will be argued that when tissues are subjected to

strains beyond linear viscoelastic levels, the nonlinear stress response leads to hysteresis type losses in response to the cyclic ultrasound stimulation. These losses ultimately appear as heat resulting from an intensity dependent absorption producing temperature rises greater than those calculated by linear extrapolation from the absorption coefficients measured at low intensity levels. At ever higher levels of ultrasound exposure, the nonlinear stress-strain response of the tissue under cyclic loading could lead to tissue mechanical fatigue failure after a number of cycles and may facilitate the initiation of cavitation events.

5.2 Finite Wave Effects

In order to facilitate finding solutions to the wave equation describing acoustic propagation, certain assumptions are made which are valid only for waves of small amplitudes. It is assumed that the magnitude of the disturbance in isotropic unbounded media is infinitesimal, e.g., the particle velocity is assumed very much smaller than the phase velocity, and that the response of the medium supporting the traveling wave is linear such that the change in density of the medium is directly proportional and in phase with the change in the pressure (Fry and Dunn, 1962). It is also assumed that the relationship between stress, strain, and their time derivatives is linear such that the material displays behavior describable by Hooke's law and Newtonian flow. The assumptions which are adequate at low intensities, and indeed correctly predict the speed with which the wave process travels through the media, fail for high intensities, particularly as energy losses are not included or predicted. Evidence exists that finite amplitude wave effects appear at relatively low levels. Fox and Wallace (1954) observed a five-fold increase in the ultrasonic absorption coefficient for water at a level of 4 W/cm^2 over that measured at 0.1 W/cm^2, due to the transfer of energy from the fundamental to harmonics, as a function of

propagation distance, and due to the consequent quadratic dependence of the absorption on frequency. Later, Beyer and Narasimham (1957) showed close agreement with Zarembo et al. (1956) and Narasimham and Beyer (1956) when α/f^2 was plotted as a function of p/f (proportional to the partiale displacement amplitude) where α is the absorption coefficient, f is the frequency (MHz) and p is the ultrasound pressure amplitude (atm). This agreement among experimenters using a wide range of intensities and frequencies implicates particle displacement as the possible parameter for nonlinear or intensity dependent absorption behavior.

For focused fields, as used in the lesion studies described herein, wave distortions due to transfer of energy to harmonics may be of little importance as the high intensities only exist over the short distances of the focal region, as was shown by calculations of Dunn and Pond (1978). However, no direct measurements have been made which would preclude the possibility of such an occurance at even higher intensities. However, when unfocused fields are employed for lesion studies, absorption measurements, or bioeffects irradiations, it should be carefully noted that the delivered intensity and the harmonic content of the wave at the site of interest may be considerably different than is usually supposed from the low intensity theory.

5.3 Nonlinear Tissue Mechanical Response

It has long been known that the stress-strain behavior of tissues deviates from the idealized Hooke's law relationship at high stress. Wertheim (1847) showed that the stress increases faster with increasing strain than predicted by Hooke's law, for static situations. Yamada (1970) compiled a very complete set of stress-strain curves for nearly all organs and tissues of the human body which showed that for static conditions, nearly all tissues exhibit a linear region

beyond which nonlinear behavior prevails which can be described by a power curve relationship $\sigma = K(\varepsilon)^n$, where σ is the stress, ε is the strain, K is a constant, and n is a positive number Similar results are obtained for dynamic conditions up to several kilohertz (McElhaney et al., 1969; Estes and McElhaney, 1970). Galford and McElhaney (1970) conducted a viscoelastic study on scalp, brain, and dura mater which showed that nonlinear stress-strain behavior also occurs at low megahertz frequency strain rates.

Figure 5-1 shows the stress-strain response typical for a wide range of tissues exhibiting a region of Hookean elasticity describable by the stress being directly proportional to the strain, i.e., $\sigma = E \cdot \varepsilon$, where E is the modulus of elasticity, and the subsequent nonlinear region for which $\sigma = K(\varepsilon)^n$, where n is a positive number.

5.3.1 Energy Dissipation Due to Nonlinear Stress-strain

For that portion of the stress-strain curve which is linear, energy which is stored under compression or tension is completely returned into the system upon the relaxation of the imposed strain. Energy is not dissipated and the system is conservative. For an applied stress amplitude exceeding the linear region, only a partial recovery of the potential energy stored by the system is returned upon removal of the external stress, with the energy loss dissipated as heat. During cyclic strain of high amplitude, hysteresis loss of energy occurs following the removal of positive and negative pressure. Hysteresis losses are characterized by a constant loss per cycle of the applied force, which may also be thought of as a loss which increases linearly with the frequency of the cyclic strain. Such an energy dissipation mechanism also yields losses which increase directly with increasing applied stress amplitude.

Such nonlinear stress-strain relationship and hysteresis loss mechanisms

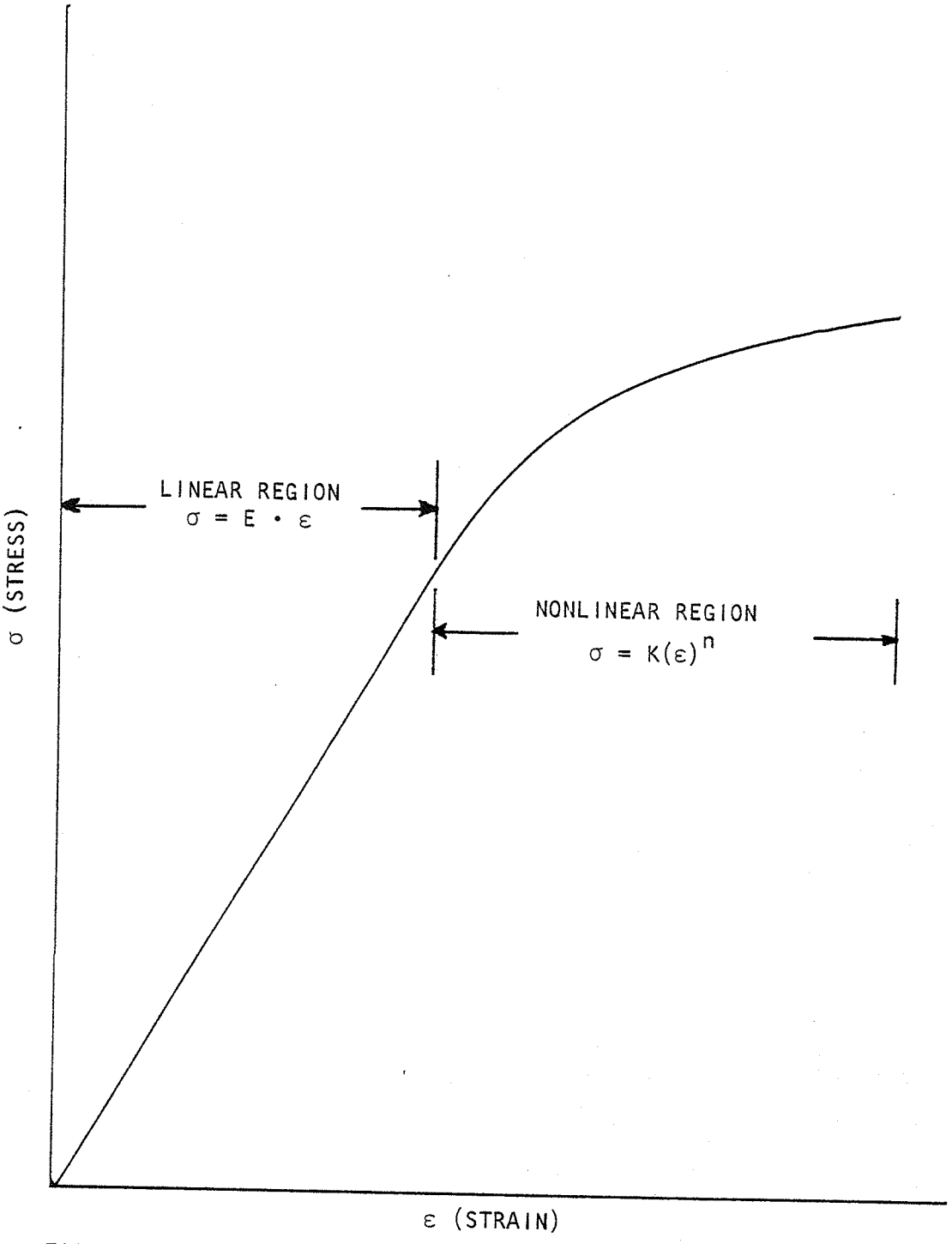

FIGURE 5-1 Stress *versus* strain typical of biological materials (Yamada, 1970) showing linear Hooke's Law and non-linear regions.

have been investigated for a wide range of materials. Litovitz and Lyon (1954) made extensive measurements in the viscous liquids glycerol and pentachlorobiphenol and found that the existing theoretical mechanisms for absorption could not describe the results obtained. Their data at high viscosities showed a frequency independent absorption loss per wavelength which they concluded could be due to the presence of a type of hysteresis. Litovitz and Lyon (1954) suggested that there may be a common origin for the hysteresis mechanism in liquids and solids. The work of Landau and Rumer (1937) showed a close correlation between ultrasonic and dielectric relaxation, wherein, above the main relaxation frequencies for dipole rotational relaxation, hysteresis effects were noted. Landau and Rumer (1937) postulated that the dielectric and acoustic hysteresis in solids and liquids have a related origin in the coupling of acoustic or electric wave energy into heat energy in the solid or liquid due to anharmonicities in the lattice structure.

Hysteresis has been studied with biological material in connection with fatigue failure of bone. Gaynor-Evans (1973) has shown that several investigators obtain nonlinear stress response curves for various bones from several species. Based on quantitative stress-strain relations, fatigue life, expressed as the number of cycles of applied cyclic strain until failure, may be predicted empirically. For example, a plot of the logarithm of the applied strain amplitude *vs* the logarithm of the number of cycles to fatigue fracture gives a straight line over several orders of magnitude (Sereg and Kempke, 1969) and is found for a great variety of solid materials.

Basquin (1910) developed a mathematical description, based on empirical observations, known as the Exponential Law of endurance tests, and subsequent elaboration and refinements have given a broader scope and firmer mathematical

foundation (Morrow, 1965; Feltner and Beardmore, 1970). Basquin's empirical approximation was $\sigma = K_1(N)^b$, where σ is the stress amplitude required to cause fatigue failure when applied for N cycles, K_1 is the stress amplitude intercept at one cycle, and b is the best fit exponent.

5.3.2 Mathematical Description

In order to correlate observed experimental results with basic physical mechanisms, it is useful to establish a more complete mathematical development than that which was used for previous empirical observations. Beginning with a generalized stress-strain relationship, integrating the energy dissipated per cycle, and assuming an energy-dependent criterion for fatigue failure, it is possible to derive a mathematical description useful for describing tissue mechanical fatigue and which may be useful for describing ultrasonic lesion threshold behavior as well.

Consider a volume of tissue subjected to a cyclic mechanical strain, as, for example, in the presence of an acoustic wave disturbance. The energy dissipated per cycle (W), is the integral of the area under the stress-strain curve since the elemental energy per unit volume is $dW = \sigma \cdot d\varepsilon$, by definition. The total area under the stress-strain curve for first quarter-cycle represents the potential energy stored during that period. During the next quarter-cycle, as the stress is removed, the path taken by the stress-strain curve for the material is assumed to be linear and parallel to the Hooke's law linear region. The area under this path represents the energy returned to the system. Thus, when the strain amplitude does not exceed the linear region, the paths are the same and no energy is dissipated by system nonlinearities.

Figure 5-2 shows a generalized stress-strain plot and the resultant hysteresis loop which would occur when the tissue sample is driven into the

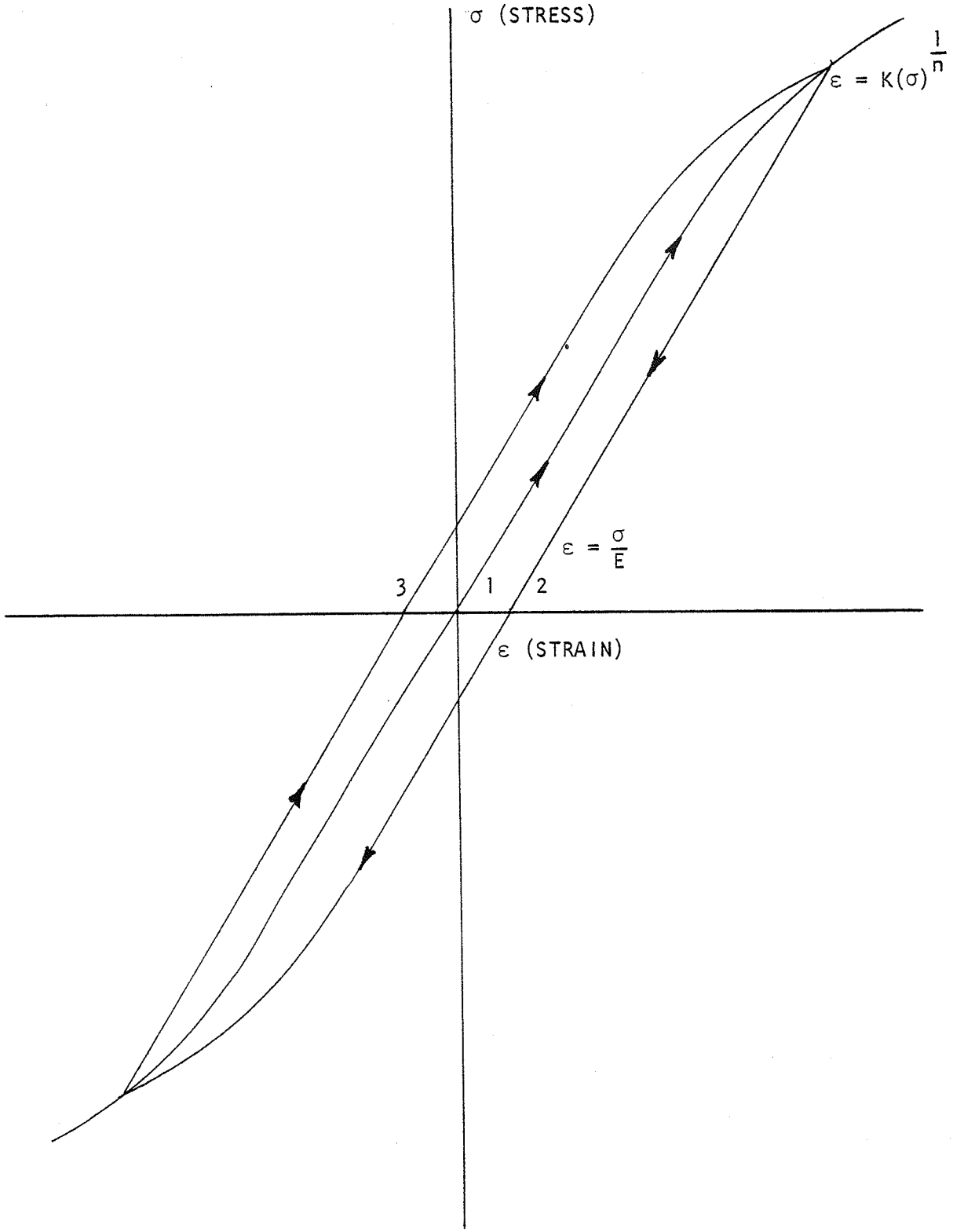

FIGURE 5-2 Full stress-strain plot showing path taken under cyclic stress and showing the resultant hysteresis loop.

nonlinear region by a cyclic external applied force. The arrows show the paths taken by the strain as the applied stress varies. Path (1) shows the first quarter-cycle and path (2) the subsequent path taken as the tissue is forcibly relaxed by the negative-going applied stress. The paths (2) and (3) show the paths taken by the subsequent positive and negative cyclic variations, assuming no alterations in stress-strain behavior due to cyclic fatigue. The area enclosed by the hysteresis loop represents the energy dissipated by system stress-strain nonlinearities for one complete cycle.

It is convenient mathematically to consider only the nonlinear region when computing the energy loss per cycle. The nonlinear region can be approximated by a power function as

$$\varepsilon = K(\sigma)^{\frac{1}{n}} \qquad (5\text{-}1)$$

The maximum energy dissipated per cycle is then

$$W = 2\int_{o}^{\sigma_a} \sigma \cdot d\varepsilon \qquad (5\text{-}2)$$

where σ_a is the maximum cyclic stress amplitude and the factor of 2 results from the symmetry of the negative half-cycle, which is assumed to be a replica of the of the positive cycle, and from the choice of limits of integration. It is convenient to consider the maximum loss case since the energy returned to the system upon relaxation of the applied stress could be any linear function of the applied force and as such can be included in the constants of integration. Differentiating equation (5-1) and substituting into the integral gives

$$W = \frac{2K}{n} \int_{o}^{\sigma_a} \sigma^{\frac{1}{n}} \, d\sigma \quad . \qquad (5\text{-}3)$$

Integration yields the energy dissipated per cycle and for N identical cycles the total energy dissipated W_N is

$$W_N = \frac{2KN}{n+1} (\sigma_a)^{\frac{1+n}{n}} \quad , \qquad (5\text{-}4)$$

This assumes no structural changes occurring and Eq. 5-1 continues to remain valid (Feltner and Morrow, 1959). If it is assumed that fatigue failure occurs after a total energy U accumulates after N_f cycles, then

$$U = \frac{2KN_f}{n+1} (\sigma_a)^{\frac{1+n}{n}} \quad . \qquad (5\text{-}5)$$

Rearranging gives,

$$\frac{U(n+1)}{2K} = N_f (\sigma_a)^{\frac{1+n}{n}} \qquad (5\text{-}6)$$

Taking the $\frac{n}{n+1}$ root and adapting the logarithmic form gives,

$$\log \sigma_a = K^1 - \frac{n}{n+1} \log N_f \quad , \qquad (5\text{-}7)$$

where $K^1 = \frac{n}{1+n} \log \frac{U(n+1)}{2K}$.

A log-log plot of maximum stress *vs* number of cycles to failure gives a straight line of slope $-\frac{n}{1+n}$ and an intercept at one cycle of $\log \sigma_a = K^1$ (Figure 5-3).

If this analysis can be applied to biological materials, and if it can be

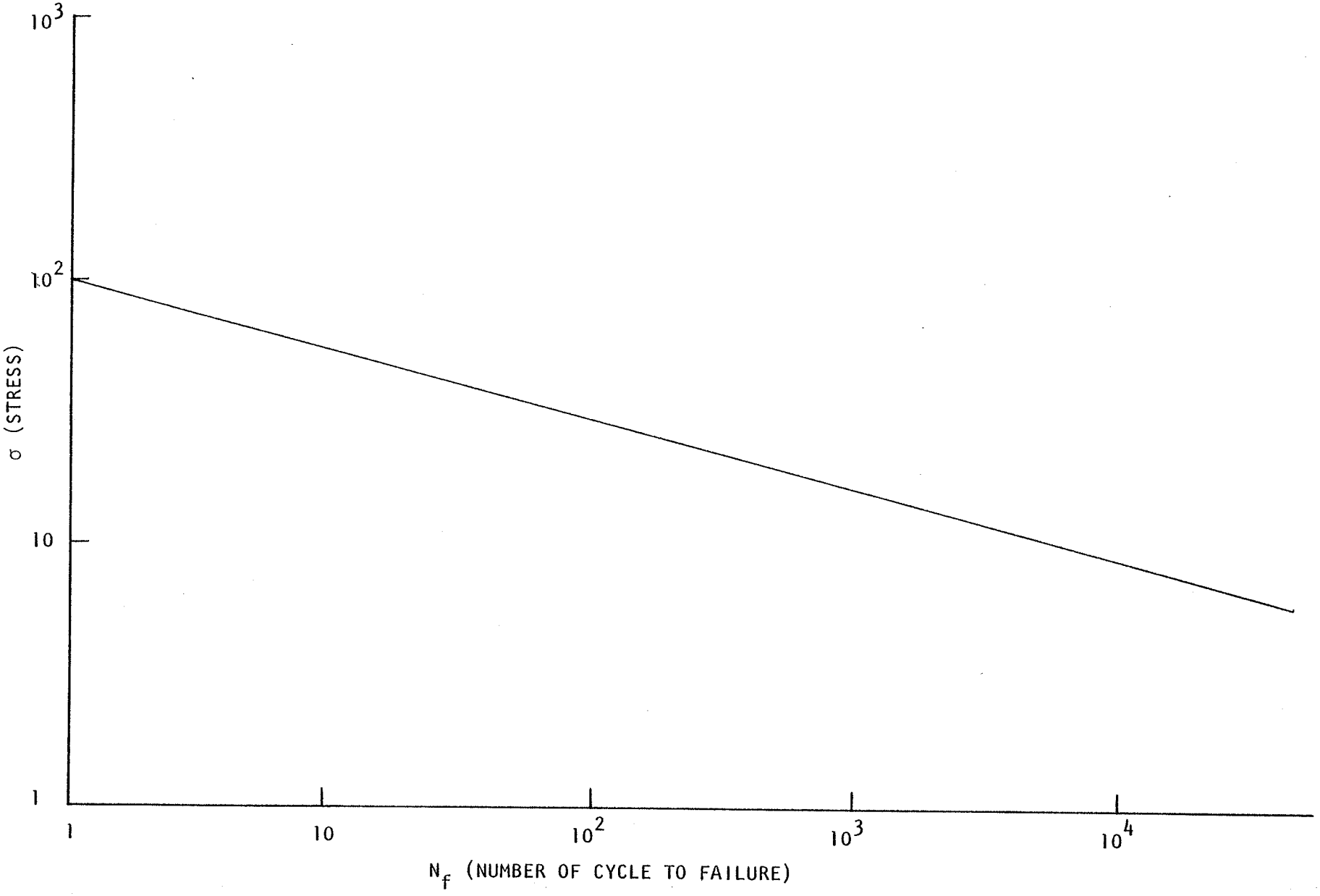

FIGURE 5-3 Stress amplitude for failure *versus* N_f (number of cycles to failure) as predicted by equation (5-7).

assumed that energy dissipated as heat by nonlinear stress-strain hysteresis contributes to the heat dissipated by other viscoeleastic absorption mechanisms during high intensity ultrasonic irradiation, then equation (5-7) may describe the kinds of events occurring during ultrasound exposures leading to irreversible structural changes. If the stress amplitude is assumed to be proportional to the ultrasonic pressure amplitude, the lesion threshold curves can be expressed as a function of the square-root of the delivered acoustic intensity. As time duration and number of cycles are linearly related by multiplying exposure duration by the frequency, the slope of the original intensity-time plot for lesion threshold (Figure 4-1) which was -1/2, on the new plot of pressure *versus* number of cycles to threshold would be -1/4. Setting this equal to the $n/(n + 1)$ in equation (5-7) gives a $n = 1/3$, which is consistent with the form of the stress-strain curves found for most biological tissues (Yamada, 1970).

Additional support for a hysteresis hypothesis may be obtained from consideration of the frequency dependence of the ultrasound absorption coefficient. For the case where no absorption is taking place, it would seem that a threshold time inversely proportional to frequency, for a given intensity, would result. For example, if 10^6 cycles were required for a lesion just to appear, at 10 MHz, it would take 10 times longer for irradiation under the same conditions at 1 MHz, for a lesion to appear. However, since μ, the intensity absorption coefficient, is nearly directly proportional to frequency, the energy absorbed at 10 MHz is ten times greater than that at 1 MHz for the same time duration. This has the effect of making the threshold curves for each frequency coincide, as was shown in Chapter 4 by the frequency correction due to the presence of brain meninges and the introduction of an impedance mismatch due to structure.

It is yet to be determined at what level of intensity such nonlinear effects become significant. Dunn (1962) measured the absorption *in vivo* in mouse spinal cord up to 175 W/cm^2 at 2°C and found no variation in absorption with intensity. The highest temperature reported was 28°C where the maximum intensity used was 75 W/cm^2. Lerner et al. (1973) gave a detailed mathematical analysis of the temperature transients produced under focused ultrasonic irradiation and found that a constant value for the absorption yielded a consistent fit to the data for lesion threshold irradiations from 1 second to over 100 seconds. On the lesion threshold curve, this would correspond to intensities of 200 W/cm^2 to less than 10 W/cm^2. Lele (1977) found an increase in absorption, as measured by the transient thermoelectric technique in *in vitro* liver (20°C), when the intensity was increased above 400-500 W/cm^2. There was approximately a doubling in the absorption coefficient in the region of 1000 W/cm^2 compared to the value measured at low intensities. Fry (1977) has measured total temperature rise for 20 second irradiations of live mouse testicle, under cw and pulsed high intensity regimes. When the data are plotted as temperature rise *vs* time-averaged intensity delivered, there appears to be a significant increase in heat dissipation for high intensity pulsed irradiations over that obtained for an equivalent (time-averaged intensity) cw case. Significant differences ($\pm$ 1/2°C) occur from about 400 W/cm^2 and above. Fry (1977) also measured the intensity absorption coefficient as a function of average intensity in live mouse testicle. For c.w. irradiations up to 120 W/cm^2, the value measured for μ was constant at about 0.04 cm^{-1}. For high intensity 50 μs bursts at 1 kHz pulse repetition rate, noticable nonlinearities were observed when intensities greater than 200 W/cm^2 were used, viz., the c.w. intensity absorption coefficient was doubled for the pulsed case at levels of about 250 W/cm^2 and reached a level of five times the low level

absorption coefficient in the neighborhood of 800 W/cm^2. All of these findings, viz., those of Dunn (1962), Lerner et al. (1973), Lele (1977), and Fry (1977) indicate thatnonlinear losses of the postulated hysteresis type appear to become important in the region of 200-1000 W/cm^2 and above.

How would the nonlinear absorption, predicted by hysteresis and observed in the above experiments, affect the proposed dosimetric quantity of absorbed dose per unit volume as approximated by the product μIt? If it is assumed that the intensity absorption coefficient increases as a function of the intensity, it could be approximated by a constant μ_o times the intensity I. The absorbed dose per unit volume would then be $\mu_o I^2 t$. In the intensity region between cavitational damage and thermal behavior, if a constant absorbed energy per unit volume (C) is required for the initation of a threshold lesion, then $\mu_o I^2 t = C$. Taking the square-root and combining constants μ_o and C^o, gives $It^{\frac{1}{2}} = C'$, which is the empirical equation describing the set of threshold curves originally obtained and as shown in Figure 4-1.

As an additional check on the validity of a hysteresis model for nonlinear ultrasound absorption, a comparison can be made of the expected levels of strain amplitudes under ultrasonic irradiation and of the strain amplitude required for the nonlinear stress response observed in a wide range of materials. Since no data are available for the measured stress-strain response for brain tissue at ultrasonic strain rates, only an order of magnitude comparison is possible. Nonlinear strain occurs at levels of micro-inches per inch in metals and ceramics (Feltner and Morrow, 1959), 10^{-3} to 10^{-2} in/in for bone and soft tissues (Yamada, 1970); Gaynor-Evans, 1973), and 0.1 in/in for elastometers (Eirich and Smith, 1972) are common. Particle displacement amplitudes for a 1000 W/cm^2, 1 MHz wave in a water-like medium are approximately $\pm$ 60 x 10^{-8} meters. Since a peak of

positive particle displacement occurs one-half wavelength away from the negative extreme, the ratio of the total displacement magnitude to the distance over which it is applied corresponds to a strain ratio of 10^{-3} meters/meter. Hence, displacement amplitudes in the intermediate intensity range for ultrasound irradiation are commensurate with strain magnitudes as observed under measured static conditions.

The hysteresis model also predicts a linearly increasing absorption *versus* increasing frequency, or a constant loss per cycle. Hysteresis was discarded as a model for absorption by previous investigators of absorption mechanisms (Hueter, 1958) since early attenuation measurements had shown that the logarithm of attenuation *versus* the longarithm of frequency had a slope of 1.5 instead of 1.0. More recent measurements of absorption by the transient thermoelectric technique have shown the slope to be very nearly unity, viz., 1.0 to 1.18 (Goss et al., 1978) for a variety of tissues including brain.

5.3.3 Hysteresis at Very High Intensities

Although the hysteresis model is proposed as a mechanism to explain lesion threshold behavior at what is considered to be sub-cavitation intensities, it is pertinent to discuss its applicability at very high intensities where cavitation can occur. The model predicts straight-line behavior of the threshold curve on a plot of the logarithm of intensity *versus* the logarithm of exposure duration for intensities and times well up into the cavitation region. The hysteresis model at intermediate level intensities was proposed as a mechanism whereby energy was dissipated at a rate in excess of what would be predicted by linear extrapolation from an acoustic absorption coefficient measured at low intensities. Hence, the primary lesion cause was thermal. At very high intensities, actual tissue mechanical fatigue failure may occur as a prelude to the initiation of subsequent cavitation, though no direct evidence for this is

available. However, it can be argued that the time delay between the beginning of high intensity ultrasonic exposure and the onset of cavitation, as measured by implanted acoustic sensors and which can be several milliseconds at 3,000 W/cm^2 (Gavrilov, 1974), could be due to the time required for a sufficient number of cycles (several thousand at MHz frequencies) to accumulate for mechanical fatigue failure to occur assuming the stress-strain behavior is similar at these higher intensities. Such modes of failure for the viscoelastic rupture of elastomers (in the absence of cavitation) have been studied extensively (Eirich and Smith, 1972), which have shown that the summation of cyclic hysteresis energy can account for such fatigue failures.

5.3.4 Hysteresis Model at Low Intensities

The model presented for hysteresis behavior is compatable with the thermal model of Pond (1968), Lerner et al. (1973), and Lele (1977) at low intensities. Indeed, the hysteresis contribution to heat production at intensities beyond which the Lerner et al. (1973) model diverges from experimental behavior (approximately 200 W/cm^2) could be used to extend the thermal models' usefulness at higher intensities. If the intensity dependent absorption predicted by the hysteresis model were used in conjunction with the thermal model, the original predicted slope of -1.0 for the threshold curves above 200 W/cm^2 would be reduced to a value much closer to the experimentally observed value of -1/2. This follows from the fact that the rate of heat production (dq/dt) due to absorption, assumed by the thermal model, which is equal to $2\alpha I$, where α is the amplitude absorption coefficient and I is the intensity of the irradiation, would be increased at higher intensities when the constant for α is replaced by $\alpha(I)$, an intensity dependent function for α. If $\alpha(I)$ is assumed to be of the form $\alpha_o + \alpha_1 I$, dq/dt becomes equal to $2\alpha_o I + 2\alpha_1 I^2$. Such intensity dependent rates

of heat production have been observed experimentally in *in vivo* mouse testicular tissue by Fry (1977), where α_T would be $\alpha_o/200$ for the 50 μs bursts.

An extension of the Lerner et al. (1973) thermal model was proposed by Carstensen et al. (1974) in which the calculated temperature transients of the previous Lerner et al. (1973) model were incorporated into an arbitary damage factor which was dependent upon the temperature, the activation energy for a thermal damage process, and the time duration of exposure. When this damage factor was integrated over the duration of the thermal transient, and reached an arbitrary value of 1.0, the intensity *versus* time for lesion production could be predicted by a suitable choice of the energy of activation used in the model. Physically realizable values for the activation energy were obtained.

However, an extension to this model is required to predict behavior for threshold lesion production in brain tissue at intensities less than 10 W/cm^2. The model predicts that a suitably long time duration of exposure at below 10 W/cm^2 would produce a lesion, which is not always the case, as Lele (1977) has shown that elevation of local brain temperature below 42.5°C does not produce morphological damage even after eight hours of exposure. Observations of similar behavior, that is, an endurance limit below which continuous application of a certain level of temperature, cyclic stress, or ultrasonic exposure does not result in damage, have been made in a wide range of materials (Eirich and Smith, 1972; Liebowitz, 1976).

5.4 Observations on Low Intensity Effects

Extended endurance or the absence of lesion production under low intensity long duration ultrasound irradiation of cat brain has been observed experimentally. Focused, low-intensity, long duration, ultrasonic exposure of the adult female cat brain has shown a marked departure from the threshold behavior which would be

predicted using the well established high intensity-time duration relationship (Dunn et al., 1975) $It^{\frac{1}{2}} = C$, where I is the intensity required to produce a lesion, t is the time duration of irradiation, and C is a constant which is weakly dependent on the frequency (Johnston and Dunn, 1976).

A total of 45 animals were irradiated at fixed intensities of 20, 15, 10, 7.5, and 5 W/cm^2 for times in the range of 20 to 1500 seconds, for a total of 160 exposures. Lesion threshold values for 20 and 15 W/cm^2 were well defined at 100 seconds and 500 seconds, respectively. However, no lesions were found for 10, 7.5, and 5 W/cm^2 irradiations for times between 250 to1500 seconds. All lesions observed were in the white matter of the brain only. Even though multiple gray matter sites were irradiated, no gray matter lesions occurred even at times 170% that of the lesion threshold time for 20 and 15 W/cm^2. The slope of the line joining the 20 and 15 W/cm^2 thresholds on a log-log plot of intensity *versus* time is approximately -1/4 as compared to the value of -1/2 which holds for over five orders of magnitude in times below 10 seconds, e.g., 10 seconds to 10^{-4} seconds.

These preliminary results of decreasing slope on the intensity-duration plot for lesion threshold, absence of gray matter lesions at 20 W/cm^2 and below, and the absence of lesions for long duration exposures at 10 W/cm^2 and below, suggest that irradiation levels may be asymptotical approaching the intensity below which no lesions can be produced for any time duration exposures. This could reflect the brain's ability to conduct heat away from the irradiation site as fast as the heat is produced by the ultrasonic irradiation. Also, during long duration exposures, there is sufficient time for additional physiological factors to influence threshold levels. Homeostatic mechanisms such as increased capillary blood flow in response to heating causes increased heat conduction away from the

irradiation site. The greater vascularity of brain gray matter coupled with its lower ultrasonic absorption coefficient explains why gray matter lesions are more difficult to produce than white matter lesions.

Empirical observations of fatigue failure in metals (Feltner and Beardmore, 1970), ceramics, elastomers (Eirich and Smith, 1972), soft tissues, and bones (Herrmann and Liebowitz, 1972) reveal a region of low amplitude strain below which failure does not occur for essentially an infinite number of cyclic stresses, e.g., in excess of 10^8 cycles. For some materials, this is due to repair mechanisms which require long times to become effective. In other systems, the dissipation of heat can account for the extended endurance since temperatures never rise above low levels. In biological systems, both may occur, but heat dissipation which holds temperature to a low level is a sufficient explanation for histologically observed lesion behavior at low intensities. Biological systems *in vivo* have additional heat dissipation capabilities which require long times to become effective for low level increases in temperature, due to blood flow and physiological accommodation. Such mechanisms which are operable only from seconds to minutes after the initiation of a heat transient, are easily excluded from consideration during high intensity, short duration exposures. The assumption that the energy absorbed at threshold is constant, which was used in the analysis at higher intensities, must be modified during long exposures at low intensities to account for energy losses due to heat convection. Similarly, the Carstensen et al. (1974) thermal model may be modified if heat losses due to blood flow perfusion of the irradiated area are included at long-time exposures.

5.5 Harmonic Production Due to Nonlinear Stress-strain

When a system is driven into a region of nonlinear behavior, harmonics are produced at integer multiples of the fundamental driving frequency. However, the generation of sub-harmonics in the acoustic case in particular at one-half the fundamental driving frequency, has been shown to be the result of small bubbles in a fluid medium being driven at twice their resonant frequency (Eller and Flynn, 1969). They showed that this phenomenon had a definite intensity threshold and could be used as a monitor for the detection of cavitation threshold. Lele (1977) performed similar measurements at megahertz frequencies in water, brain, and liver and found the presence of half harmonic signals at levels well below the threshold for collapse cavitation down to levels of a few tenths of a Watt per square centimeter. There appeared to be a transition region at the level of collapse cavitation at about 1500 W/cm^2 where the strength of the sub-harmonic increased rapidly. But no threshold for the half-harmonic was seen at low intensities. Neppiras (1969) noted that it had been observed that half-harmonic signals could occur in the absence of bubbles and cited the work of Tucker (1965) and Dunn, G. J. et al. (1965). These investigators had found that strong half-harmonic signals might be generated due to the nonlinear compliance of the medium and the presence of bubbles was not always necessary for the observation of half-harmonic signals. They stated additionally, that the nonlinear compliance of the system would explain only the half-harmonic signals. It is postulated here, with additional evidence, that the half-harmonic signal levels measured by Lele (1977) could be explained by the work of Friedel (1964) and Peguin et al. (1967) wherein it is shown that the strain velocity (time rate of change of the strain) in a nonlinear system increases with the hyperbolic-sine of the applied stress. If the measurements of Lele (1977) were to be repeated as a

function of temperature, the half-harmonic signal strengths observed may be predicted on the basis of the strain velocities and their dependence on temperature as shown by Friedel (1964). The experimental measurements of half-harmonic signals at orders of magnitude below transient collapse cavitation intensities is offered not only as possible evidence of behavior which is a predictable consequence of the nonlinear stess-strain hysteresis model, but also as a source of future investigation of nonlinear tissue mechanical behavior, as was cited above.

5.6 Hysteresis and Ultrasound Absorption and Velocity Dispersion

It is instructive to compare the frequency dependences of absorption and velocity as predicted by a hysteresis mechanism with those predicted by shear viscosity and relaxational mechanisms. The absorption per unit path length is directly and linearly proportional to frequency for the hysteresis model since there is a constant loss per cycle of the applied stress. The frequency dependence of absorption predicted by shear viscosity (Fry and Dunn, 1962) indicates that the absorption should increase as the square of the frequency with a transition at frequencies in excess of 10^8 Hz (predicted for soft tissues) where there should occur a transition to square-root dependence on frequency. At those frequencies, the velocity dependence on frequency should also go through a transition from no dependence upon frequency (no dispersion) to a dependence directly porportional to the square root of the frequency. For a relaxation mechanism low frequency absorption is predicted to be directly proportional to the square of the frequency. Above the relaxation frequency, absorption becomes constant. Velocity is predicted to be constant below the relaxation frequency (no dispersion), then goes through a transition region at the relaxation frequency (displays some dispersion), and above the characteristic relaxation

frequency assumes a fixed value (no dispersion) at a velocity which is greater than the low frequency value.

Hysteresis, as was proposed by Mason and McSkimmin (1947) for metals and glasses, and the mathematical development for it proposed by Mason (1950), yielded a frequency independent value for velocity. Although Mason and McSkimmin (1947) and Litovitz and Lyon (1954) conducted hysteresis absorption studies in metal, glass, and viscous liquids, no velocity data was obtained. No measurable dispersion has been observed in homogeneous biological tissues. Dispersion in non-homogeneous tissues such as lung (Dunn, 1974) and bone (Yoon and Katz, 1976) has been observed

Care must be taken in dispersion measurements in tissues to exclude group-velocity dispersion due to frequency-dependent boundary impedances which may interfere with velocity measurements as demonstrated by Lange (1966). Further, the measurement of a frequency dependent variation in velocity which would contradict the dispersion-free velocity prediction of the hysteresis model may have to be conducted at intensity levels where hysteresis is proposed to predominate as a nonlinear effect (several hundred Watts per square centimeter).

Chapter 6

SUMMARY

In Chapter 3, a dose-effect relationship was demonstrated to exist between the absorbed energy per unit volume and the produced lesion volume. The units of the proposed dosimetric quantity are joules per cubic millimeter and is approximated by the product of the intensity absorption coefficient (μ), the delivered intensity (I) at the lesion site, and the duration of the exposure (t). The dose-effect relationship was obtained for various combinations of the involved exposure parameters (μ, I, and t) and it emerged that the observed biological effect, viz., a given lesion volume at any given dose-rate, could be obtained by equivalent absorbed doses at two different irradiation frequencies. It was suggested that a universal set of such curves, as were presented for brain tissue, could be obtained by other investigators using other tissues.

It was shown in Chapter 4 that the frequency dependent attenuation of the collagenous brain meninges could account for the frequency variations, in the threshold for lesion production in the brain parenchyma, observed earlier. An additional minimum in attenuation was predicted at 7 MHz by a three layered model of the brain meninges, and subsequent lesion threshold experiments yielded results compatible with the presence of such a minimum. The results of the section showed that the lesion threshold in the brain tissue itself is frequency independent at about 200 W/cm^2 for a 1 second duration exposure. These results are useful in the dosimetry, since it resolves frequency differences for lesion threshold and helps to refine values for delivered intensities by correcting for

reflections and attenuation at the brain meninges.

In Chapter 5 mechanisms for ultrasound bioeffects were considered and the mechanism of hysteresis was proposed for high intensity level ultrasound bioeffects. Starting with the known nonlinearities of tissues subjected to high levels of stress and integrating the energy dissipated over many cycles of the alternating applied stress, it was possible to arrive at a description of the hysteresis losses so generated. When the model of the hysteresis losses was applied to ultrasonic lesion production in brain tissue, the required value used by the model for the description of the tissue nonlinearity corresponded to values which had been measured for brain tissue, thus lending support to the view that hysteresis must be considered seriously as a mechanism for the observed biological effect.

Chapter 7

CONCLUDING REMARKS

If radiation protection guidelines are to be established for human exposures to ultrasound as used in medical diagnostics, therapy, and surgery, dosimetric quantities must be established which are adequately descriptive of the exposure levels reponsible for the biological effects. The dosimetric quantity must show a predictive behavior by indicating the expected threshold for the appearance of the biological effect and above threshold must show a quantitative behavior by a definite covariance with the magnitude of the observed bioeffect. The results of Chapter 3 demonstrate that absorbed energy per unit volume satisfies these criteria for continuous wave irradiations at levels typical of therapeutic and surgical intensities. Additional research is required for the pulsed regimes and low intensities which are used at diagnostic levels to determine what additional dosimetric considerations are necessary.

In addition to the effects of ultrasound on tissues, consideration must be given for research on the effects of tissues on the propagation of ultrasound. Chapter 4 showed that refinements in dose determination could be made when corrections for the attenuation and reflection of ultrasound by biological tissues were considered. It is necessary to determine closely the intensity delivered to the site of interest.

Even though the hysteresis model was presented as a mode of heat production in excess of that calculated by extrapolation from an acoustic absorption coefficient measured at low intensities, the model may also hold at intensities where cavitation is likely to occur. Future research should consider that the time

required for the onset of cavitation may be a reflection of the number of cycles required for hysteresis energy to accumulate to a level of which tissue mechanical fatigue failure occurs.

It was also shown that the hysteresis model was consistent with existing thermal models for lesion production at low intensities. It may be possible that the hysteresis losses may be used to extend the region for which the thermal models closely follow experimental observations by inclusion of the predicted intensity dependent absorption. Also, the existence of an intensity dependent absorption is important for comparing bioeffects data, with differing exposure conditions, on the basis of time-averaged and spatial-averaged intensities. As demonstrated by the results for temperatures produced in live mouse reproductive organs (Fry, 1977), pulsed high intensity irradiation produced temperatures which far exceeded c.w. exposures even though time-averaged intensities were equivalent. Future bioeffects data should report spatial-peak and temporal-peak intensities if meaningful intercomparisons of biological effects experiments are to be made. Many of the consequences of hysteresis behavior may have already been observed. Nonlinear or intensity dependent absorption has been seen in brain and mouse testicle. The linear increase in absorption with frequency has also been noted in a wide variety of tissues. Harmonic and subharmonic production of an intensity dependent nature has also been noted at low levels. Another consequence of hysteresis, frequency independent ultrasonic velocity, has been observed in all tissues measured, except for lung and bone. Further velocity measurements as a function of frequency are needed.

It is hoped that nonlinear tissue mechanical response and hysteresis loss mechanisms at ultrasonic frequencies will be of benefit in supplying future impetus for research into the consequences of these mechanisms in ultrasonic

biophysics. It is also hoped that the dose-effect relationships presented and their quantitative description in terms of absorbed energy per unit volume will form the basis of future dosimetric work.

REFERENCES

Barnard, J. W., Fry, W. J., Fry, F. J., and Krumins, R. F. (1955). "Effects of High Intensity Ultrasound on the Nervous System of the Cat," J. Comp. Neurol. 103, 459-484.

Barnard, J. W., Fry, W. J., Fry, F. J., and Brennan, J. F. (1956). "Small Localized Ultrasonic Lesions in the White and Gray Matter of the Cat Brain," Arch. Neurol. and Psychiat. 75, 15-35.

Basauri, K. and Lele, P. P. (1962). "A Simple Method for Production of Trackless Focal Lesions with Focused Ultrasound: Statistical Evaluation of the Effects of Irradiation on the Central Nervous System of the Cat," J. Physiol. 160, 513-534.

Basquin, O. H. (1910). "The Exponential Law of Endurance Tests," Proceedings Am. Soc. Testing Mats. 10, Part II, 625-630.

Beyer, R. T. and Narasimhan V. (1957). "Note on Finite Amplitude Waves in Liquids," J. Acoust. Soc. Am. 29, 532.

Brown, R. E. (1971). "Uses of Ultrasound in Diagnosis," in Interaction of Ultrasound and Biological Tissues Workshop Proceedings, DHEW (FDA) 73-8008, BRH/DBE 73-1, U. S. Govt. Printing Office, Washington, DC, p. 221.

Carstensen, E. L., Miller, M. W., and Linke C. (1974). "Biological Effects of Ultrasound," J. Biol. Phys. 2 (4), 173-192.

Dunn. F. (1958). "Physical Mechanisms of the Action of Intense Ultrasound on Tissue." Am. J. Phys. Med. 37 148-151.

Dunn, F. (1962). "Temperature and Amplitude Dependence of Acoustic Absorption in Tissue," J. Acoust. Soc. Am., 34, 1545-1547.

Dunn, F. (1974). "Attenuation and Speed of Ultrasound in Lung," J. Acoust. Soc. Am. 56, 1638-1639.

Dunn, F. and Brady, J. K. (1974). "Pogloshchenie Ul'trazvyeka V Biologicheskikh Sredakh (Ultrasonic Absorption in Biological Media)," Biofizika 18, 1063-1066 (1973). (Russian, English abstract) trans. Biophysics 18, 1128-1132.

Dunn, F. and Brady, J. K. (1974). "Temperature and Frequency Dependence of Ultrasonic Absorption in Tissue," Proc. 8th Int'l. Congress on Acoustics, Goldcrest Press I (Trowbridge, Wilts, 1974), p. 366c.

Dunn, F. and Fry, F. J. (1971). "Ultrasonic Field Measurement Using a Suspended Ball Radiometer and Thermocouple Probe," Workshop Proceedings, Interaction Ultrasound and Biological Tissues, Seattle, WA, DHEW #73-8008, p. 173.

Dunn, F. and Pond, J. B. (1978). "Selected Non-Thermal Mechanisms of Interaction of Ultrasound and Biological Media," in Ultrasound: It Applications to Medicine and Biology, Part II, F. J. Fry, ed., Elsevier Scientific Publishing Co., New York, p. 539.

Dunn, F., Lohnes, J. E., and Fry, F. J. (1975). "Frequency Dependence of Threshold Ultrasonic Dosages for Irreversible Structural Changes in Mammalian Brain," J. Acoust. Soc. Am. 58, 512-514.

Dunn, G. J., Kuljis, M., and Welsby, V. G. (1965). "Non-linear Effects in a Focused Underwater Standing Wave Acoustic System," J. Sound. Vibration. 2, 471-476.

Dussik, K. T. and Fritch, D. J. (1956). "Determination of Sound Attenuation and Sound Velocity in the Structure Constituting the Joints and of the Ultrasonic Field Distribution within the Joints of Living Tissues and Anatomical Preparation, both in Normal and Pathological Conditions," Public Health Service, Nat'l. Inst. Health Project A-454, Prog. Rep. (15 Sept., 1956).

Eirich, F. R. and Smith, T. C. (1972). "Isothermal Rupture of Elastomers," in Fracture: An Advanced Treatise, Vol. 7, ed. by H. Liebowitz, Academic Press, New York.

Eller, A. and Flynn, H. G. (1969). "Generation of Subharmonics of Order One-half by Bubbles in a Sound Field," J. Acoust. Soc. Am. 46, 722-727.

Esche, R. (1952). "Untersuchung der Schwingungskavitation in Flüssigkeiten," Acoustics, 2AB, 208-218.

Ester, M. S. and McElhaney, J. H. (1970). "Response of Brain Tissue to Compressive Loading," Am. Soc. Mech. Engr., paper No. 70-BHF-13.

Feltner, C. E. and Beardmore, P. (1970). "Strengthening Mechanisms in Fatigue," in Achievement of High Fatigue Resistance in Metals and Alloys, ASTM STP 467, Am. Soc. Testing and Materials 77-112.

Feltner, C. E. and Morrow J. (1959). "Micro-plastic Strain Hysteresis Energy as a Criterion for Fatigue Fracture," TAM Report No. 576, Department of Theoretical and Applied Mechanics, Univ. of Illinois, May 1959.

Fields, S. and Dunn, F. (1973). "Correlation of Echographic Visualizability of Tissue with Biological Composition and Physiological State," J. Acoust. Soc. Am. 54, 809-812.

Fox, F. E. (1940). "Sound Pressure on Spheres," J. Acoust. Soc. Am. 12, 147-149.

Fox, F. E. and Wallace, W. A. (1954). "Absorption of Finite Amplitude Sound Waves," J. Acoust. Soc. Am. 26, 994-1006.

Friedel, J. (1964). Dislocations, Pergraman Press, Oxford, p. 211-228.

Fry, F. J. and Dunn F. (1972). "Interaction of Ultrasound and Tissue," in Interaction of Ultrasound and Biological Tissue. Workshop Proceedings Battelle Seattle Research Center, Seattle, WA, November 8-11, 1971, U. S. Department of Health, Education and Welfare.

Fry, F. J., Kossoff, G., Eggleton, R. C., and Dunn, F. (1970). "Threshold Ultrasonic Dosages for Structural Changes in Mammalian Brain," J. Acoust. Soc. Am. 48, 1413-1417.

Fry, F. J., Johnson, L. K., Erdmann, W. A., and Baird, A. I. (1977). "Ultrasound Toxicity in the Mouse," in Symposium on the Biological Effects and Characterizations of Ultrasound Sources, HEW Publication (FDA) 78-8043, p. 153-164.

Fry, W. J. (1958). "Intense Ultrasound in Investigations of the Central Nervous System," in Advances in Biological and Medical Physics, Vol. VI, Academic Press Inc., New York, p. 282-348

Fry, W. J. and Dunn, F. (1962). "Ultrasound: Analysis and Experimental Methods in Biological Research," in Physical Techniques in Biological Research, Vol. 4, Chap. 6, W. L. Nostuk, ed., Academic Press, Inc., New York, p. 261-394.

Fry, W. J. and Fry, R. B. (1954a). "Determination of Absolute Sound Levels and Acoustic Absorption Coefficients by Thermocouple Probes--Theory," J. Acoust. Soc. Am. 26, 294-310.

Fry, W. J. and Fry, R. B. (1954b). "Determination of Absolute Sound Levels and Acoustic Absorption Coefficients by Thermocouple Probes--Experiment," J. Acoust. Soc. Am. 26, 311-317.

Fry, W. J., Wulff, V. J., Tucker, D., and Fry, F. J. (1950). Physical Factors Involved in Ultrasonically Induced Changes in Living Systems: I. Identification of Non-temperature Effects," J. Acoust. Soc. Am. 22, 867-876.

Fry, W. J., Mosberg, J., W. H., Barnard, J. W., and Fry, F. J. (1954). "Production of Focal Destructive Lesions in the Central Nervous System with Ultrasound," J. Neurosurg. 11, 471-478.

Fry, W. J., Barnard, J. W., Fry, F. J., and Brennan, J. F. (1955). "Ultrasonically Produced Localized Selective Lesions in the Central Nervous System," Am. J. Phys. Med. 34, 413-423.

Fung, Y. B. (1972). "Stress-Strain History Relations of Soft Tissues in Simple Elongation," in Biomechanics: Its Foundation and Objectives, ed. by Y. C. Fung and M. Anliker, Prentice Hall, New Jersey, p. 181-208.

Galford, J. E. and McElhaney, J. H. (1970). "A Viscoelastic Study of Scalp, Brain, and Dura," J. Biomech. 3, 211-222.

Gaynor Evans, F. (1973). Mechanical Properties of Bone, Charles C. Thomas, Springfield, IL.

Gavrilov, L. R. (1974). "Physical Mechanism of the Lesion of Biological Tissues by Focused Ultrasound," Sov. Phys. Acoust. 20, 16-18.

Goss, S. A. (1978). The Role of Collagen in the Ultrasonic Properties of Collagen. Ph.D. Thesis, University of Illinois, Urbana, IL.

Goss, S. A., Johnston, R. L., and Dunn, F. (1978). "Comprehensive Compilation of Empirical Ultrasonic Properties of Mammalian Tissues," J. Acoust. Soc. Am. 64, 423-457.

Gould, R. K. and Coakley, W. T. (1974). "The Effects of Acoustic Forces on Small Particles in Suspension," in Finite-Amplitude Wave Effects in Fluids, L. Bjorno, ed., I.P.C. Science and Technology Press, p. 252-257.

Hasegawa, T. and Yosioka, K. (1969). "Acoustic Radiation Force on a Solid Elastic Sphere," J. Acoust. Soc. Am. 46, 1139-1143.

Herrmann, G. and Liebowitz, H. (1972). "Mechanics of Bone Fracture," in Fracture: An Advanced Treatise, Vol. 7, Academic Press, New York, p. 772.

Heuter, T. F. (1958). "Viscoelastic Losses in Tissues in the Ultrasonic Range," Wright Air Development Center Technical Report (WADC-TR-57-706) August 1958, Contract AF 33(616)-2976.

Hodgman, C. D. (1954). C.R.C. Standard Mathematical Tables, Twelfth Edition, Chemical Rubber Publishing Co., Cleveland, Ohio, p. 402.

Hulmes, D. J. S., Miller, A., White, S., and Doyle, B. B. J. (1977). "Interpretation of the Meridional X-ray Diffraction Pattern from Collagen Fiber in Terms of Known Amino Acid Sequence." J. Molec. Biol. 110, 643-666.

Johnston, R. L. and Dunn, F. (1976). "Ultrasonic Absorbed Dose, Dose Rate, and Produced Lesion Volume," Ultrasonics 14, 153-155.

Johnston, R. L. and Dunn, F. (1976). "Influence of Subarachnoid Structures on Transmeningeal Ultrasonic Propagation," J. Acoust. Soc. Am., 60, 1225-1227.

Kinsler, L. and Frey, A. (1962). Fundamentals of Acoustics, John Wiley and Sons, Inc., New York, p. 136-139.

Kossoff, G. (1972). "Improved Techinques in Ultrasonic Cross Section Echography," Ultrasonics 10, 221-228.

Landau, V. L. and Rumer, G. (1937). Physik. Z. Sowjetunion 11, 18.

Landgraf, R. W. (1973). "Cumulative Fatigue Damage Under Comples Strain Histories," in Cyclic Stress-Strain Behavior, A.S.T.M. STP 519, Am. Soc. Testing and Materials, 213-228.

Lange, J. N. (1966). "Group Velocity Dispersion Due to Pulse Reflection from a Frequency Dependent Boundary Impedance," J. Acoust. Soc. Am. 40, 998-1001.

Lehmann, J. F. and Guy, A. W. (1972). "Ultrasound Therapy," in Interaction of Ultrasound and Biological Tissues Workshop Proceedings, ed. J. M. Reid and M. R. Sikov, DHEW (FDA) 73-8008, BRH/DBE 73-1, U. S. Governemtn Printing

Office, Washington, DC, p. 141.

Lehmann, J. F., Warren, C. G., and Guy, A. W. (1978). "Therapy with Continuous Wave Ultrasound," in Ultrasound: Its Applications in Medicine and Biology, Part I, ed. F. J. Fry, Elsevier Scientific Co., New York, p. 561.

Lele, P. P. (1977). "Thresholds and Mechanisms of Ultrasonic Damage to 'organized' Animal Tissues," Presented at the Symposium on Biological Effects and Characterizations of Ultrasound Sources, Rockville, MD, June 1977, HEW Publication (FDA) 78-8048, 224-239.

Lele, P. P. and Pierce, A. D. (1972). "The Thermal Hypothesis of the Mechanism of Ultrasonic Focal Destruction in Organized Tissue," in Interaction of Ultrasound and Biological Tissues Proceedings of Workshop, Battelle, Seattle Research Center, Seattle, WA, November 8-11, 1971, U. S. Dept. of Health, Eduction and Welfare.

Lerner, R. M., Carstensen, E. L., and Dunn, F. (1973). "Frequency Dependence of Thresholds for Ultrasonic Production of Thermal Lesions in Tissue," J. Acoust. Soc. Am. 54, 504-506.

Lillie, R. D. (1954). Histopathologic Technic and Practical Histochemistry, Blackston Co., Inc. New York, p. 330.

Litovitz, T. A. and Lyon, T. (1954). "Ultrasonic Hysteresis in Viscous Liquids," J. Acoust. Soc. Am. 26, 577-580.

Litovitz, T. A. Lyon, T., and Peselnick, L. (1954). "Ultrasonic Relaxation and its Relation to Structure in Viscous Liquids," J. Acoust. Soc. Am. 26, 566-576..

Lockhart, R. D., Hamilton, G. F. and Fyfe, F.W. (1972). Anatomy of the Human Body, J. B. Lippincott Co., Philadelphia.

Marx, J. L. (1974). Diagnostic Medicine, Science 186, 247-250.

Mason, W. P. (1950). Piezoelectric Crystals and their Application to Ultrasonics, Van Nostrand, New York, p. 431.

Mason, W. P. and McSkimmin, H. J. (1947). "Attenuation and Scattering of High Frequency Sound Waves in Metals and Glasses," J. Acoust. Soc. Am. 19, 464-473.

McElhaney, J. H., Stalnaker, R. L., Ester, M. S., and Rose, L. S. (1969). "Dynamic Mechanical Properties of Scalp and Brain," Proceedings of the 6th Annual Rocky Mountain Bioengineering Symposium, Laramie, p. 67-73.

Meyers, R., Fry, W. J., Fry, F. J., Dreyer, L. L., Schultz, D. F., and Noyes, R. F. (1959). "Early Experiences with Ultrasonic Irradiation of the Pallidofugal and Nigral Complexes in Hyperkinetic and Hypertonic Disorders," J. Neurosurg. 16, 32-54.

Morrow, J. (1965). "Internal Friction, Damping, and Cyclic Plasticity," A.S.T.M. STP 378, Am. Soc. Testing and Materials, 45-84.

Narasimhan, V. and Beyer, R. T. (1956). "Attenuation of Ultrasonic Waves of Finite Amplitude in Liquids," J. Acoust. Soc. Am. 28, 1233-1236.

Neppiras, E. A. (1969). "Subharmonic and Other Low-frequency Emissions from Bubbles in Sound-irradiated Liquids," J. Acoust. Soc. Am. 46, 587-601.

Nyborg, W. L. (1978). "Physical Mechanisms of Biological Effects of Ultrasound," HEW Publication (FDA) 78-8062.

O'Brien, Jr., W. D. (1978). "Ultrasonic Dosimetry," in Ultrasound: Its Application in Medicine and Biology, Part 1, F. J. Fry, ed., Elsevier Scientific Publishing Co., New York, p. 343.

Peqiun, P., Perez, J., and Gobin, P. (1967). "Amplitude Dependent Path of the Internal Friction of Aluminum," Trans. Metal Soc., AIME, 239, 438-457.

Pond, J. B. (1968). "A Study of the Biological Action of Focussed Mechanical Waves (Focussed Ultrasound)," Ph.D. Thesis, University of London.

Pond, J. B. (1969). The Role of Heat in the Production of Ultrasound Focal Lesions," J. Acoust. Soc. Am. 47, 1607-1611.

Qaustel, J. H. (1961). The Chemistry of Brain Metabolism in Health and Disease, Charles C. Thomas, Springfield, Illinois, p. 37-45.

Ranson, S. and Clark S. (1959). The Anatomy of the Nervous System, Saunders, London, p. 72-73.

Robinson, T. C. and Lele, P. P. (1972). "An Analysis of Lesion Development in the Brain and in Plastics by High-Intensity Focused Ultrasound at Low-Megahertz Frequencies," J. Acoust. Soc. Am. 51, 1333-1351.

Seireg, A. and Kempke, R. (1969). "Behavior of *in vivo* bone under Cyclic Loading," J. Biomech, 2, 455-461.

Siegmund, O. H. (1961). The Merck Veterinary Manual, Merck and Co., New Jersey, p. 1520.

Smith, S. W. (1976). "Diagnostic Equipment and Its Use," Eighth Annual National Conference on Radiation Control, May 2-7 (1976), Springfield, IL.

Stratmeyer, M. E. (1977). "Research Directions in Ultrasound--A Public Health View," in Symposium on Biological Effects and Characterizations of Ultrasound Sources Proceedings, HEW (FDA) 78-8048, p. 240-245.

Taylor, K. J. W. and Newman, D. I. (1972). "Electrophoretic Mobility of Ehrlich Cell Suspensions Exposed to Ultrasound of Varying Parameters," Phys. Med. Biol. 17, 98-112.

Thompson, S. W. (1966). Selected Histochemical and Histopathological Methods, Charles S. Thomas, Springfield, Illinois, p. 351.

Tucker, D. G. (1965). "The Exploitation of Non-linearity in Underwater Acoustics," J. Sound Vibration, 2, 429-434.

Weed, L. H. (1934). "Certain Anatomical and Physicological Aspects of the Meninges and Cerebrospinal Fluid," Brain, 58, 383-397.

Wertheim, M. G. (1847). "Memoire sur l'elasticite et la Cohesion des Principaux Tissus du Corps Humain," Annales de Chimie et de Physique Paris, Ser 3, Vol. 21, 385-414.

Yamada, H. (1970). Strength of Biological Materials, Williams and Wilkins Co., Baltimore.

Yoon, H. S. and Katz, J. L. (1976). "Dispersion of the Ultrasonic Velocities in Human Cortical Bone," 1976 Ultrasonic Symp. Proc., IEEE Cat. No. 76-CH1120-5SU, p. 48-50.

Zarembo, L. K., Krasil'nikov, V. A., and Shklovskaia-Kordi, V. V. (1956). "The Distortion of Ultrasonic Waves of Finite Amplitude in Liquids," Doklady Akad. Nauk. SSSR, 109, 731.

APPENDIX

DATA TABULATION

FOR 7 MHz THRESHOLD

$It^{\frac{1}{2}}(W/cm^2/sec^{\frac{1}{2}})$
206
191
179
178
171
170
156
125

MEAN = 172.0

STANDARD DEVIATION = 46.2

VITA

Ronald Lee Johnston was born in Moline, Illinois, December 12, 1944. He completed primary and secondary education in Rock Island, Illinois, graduating from Rock Island Senior High School in 1962. He entered the University of Illinois in 1962, majoring in physics with a mathematics minor. In 1967, he accepted a full-time position as a Nuclear Accelerator Engineer at the Nuclear Radiations Laboratory of the University of Illinois. From 1968 to 1972, he served in Korea and Japan in the Army Branch of the National Security Agency as a Korean Language Specialist with secondary language responsibilities in Russian, Chinese, and French. He returned to the University of Illinois in 1972, received the B.S. degree in Physics in 1973, and the same year, entered graduate school in the Department of Physiology and Biophysics. From 1974 until receiving his Ph.D. he was a Graduate Research Assistant in the Bioacoustics Research Laboratory of the Department of Electrical Engineering at the University of Illinois. He is the coauthor of seven papers in the field of Ultrasonic Biophysics.